Wheel-rail contact simulation with lookup tables and KEC-equivalent profiles: A comparative study

José L. Escalona[a], Xinxin Yu[b], Javier F. Aceituno[c,*]

[a] *Dept. of Mechanical and Manufacturing Engineering, University of Seville (Spain)*

[b] *Dept. of Mechanical Engineering, LUT University (Finland)*

[c] *Dept. of Mechanical and Mining Engineering, University of Jaén (Spain)*

Abstract

This paper describes and compares the use of two constraint-based formulations for the wheel-rail contact simulation in multibody dynamics; (1) the use of contact lookup tables and (2) the Knife-edge Equivalent Contact constraint method (KEC-method). Both formulations are presented and an accurate procedure to interpolate within the data in the lookup table is also described. Since the wheel-rail constraint contact approach finds difficulties at simultaneous tread and flange contact scenarios, the lookup table method is implemented with a penetration-based elastic contact model for the flange, turning the method into a hybrid (constant in the tread and elastic in the flange) approach. To deal with the 2-point contact scenario in KEC-method, a regularisation of the tread-flange transition allows the use of the constraint approach in the tread and also in the flange. To show the applicability and limitations of both methods, they are studied and compared with special emphasis in the calculation of normal and tangential contact forces. Numerical results are based on the simulation of a two-wheeled bogie vehicle in different case studies that consider irregular tracks and two wheel-rail profiles combination: profiles that do not show two-point wheel-rail contacts and profiles that show two-point contacts. Although results show a good agreement between both approaches, the use of the KEC-method is more extensive since it allows to reproduce the wheel-climbing scenario that cannot be simulated with the lookup table and hybrid contact approach. It is concluded that simulations with this later method may not be in the safe side.

Keywords: Contact lookup table, KEC-method , Interpolation, Wheel-rail contact, Wheel-climbing

1. Introduction

In multibody dynamic simulation of railway vehicles, the modelling of wheel-rail contact plays a fundamental role through the literature. Contact forces and their locations within wheel and rail profiles highly influence in the dynamic behaviour of the vehicles. Hence, the development of contact

*Corresponding author

Email addresses: escalona@us.es (José L. Escalona), xinxin.yu@lut.fi (Xinxin Yu), jaceitun@ujaen.es (Javier F. Aceituno)

models in terms of accuracy and efficiency is of great interest for the research community [1, 2, 3]. Among these works, two well-known approaches are commonly used to simulate wheel/rail contact in multibody railway simulations. The first one is the elastic approach, in which interpenetration and separation between the wheel and rail surfaces is allowed and normal contact forces are computed, for example, using a Hertzian-based model that calculates normal contact forces using the interpenetration and interpenetration rate [4, 5, 6]. The second one is the constraint approach, where the contact between wheel and rail is computed by solving a set of nonlinear constraint equations that establish that both surfaces in contact coincide in one or more singular contact points without penetration or separation [7, 8]. In this approach, normal contact forces are described through the Lagrange multipliers, which are associated with the contact constraints at each contact point.

One main difference between the elastic and the constraint approach is the need of a contact-point search. The elastic method always need a contact search. However, the constraint method does not need it if the location of the contact points is determined with surface parameters that are considered as non-generalised coordinates of the system and integrated forward in time.

In this sense, two methodologies can be used for the contact search. On the one hand, this search can be addressed using the *online* method. In this approach, the location of the contact points is determined at each time step of the dynamic simulation by solving a set of algebraic nonlinear equations that evaluates the contact points as a function of the wheelset-track relative position. Many works can be found in the literature that use the online search method. In this sense, Marques et al. [9] present an approach to determine contact points in the conformal zone between wheel tread and flange, based on the evaluation of the contact between each wheel strip and rail avoiding inaccuracies of the minimum distance method. Magalhães et al. [10] proposed an elastic contact model for non-Hertzian conditions providing accurate results and efficient simulations. In the work of Pombo and Ambrósio, it is proposed a three dimensional online contact detection approach to analyse the lead/lag flange contact scenarios [11], small radius track simulation [12] and the inclusion of track irregularities [13]. In the work of Malvezzi et al. [14], two contact elastic detection methods are proposed with the known analytical expressions of the wheel and rail surfaces, one is based on the idea of minimising the distance another is minimising the difference between the surfaces. Both methods are giving efficient computational times and good agreement in terms of kinematic variables and contact forces between Matlab and Simpack Rail models in [15]. Also, Baeza et al. [16] proposed a elastic detection approach to calculate the inter-penetration areas between wheel and rail. In their work, the geometries of the wheel surface are discretised by using cones and rail head by using knife-edge lines. Moreover, in the goal of reducing the computational cost of online contact search methods, Muñoz et al. [17] presents a multibody model of railway vehicles that uses simplified contact constraints for the online wheel-tread solution combined with an elastic approach for the flange. In the same context, Escalona et al. [18] presents the simplified constraint-based wheel-rail contact method called KEC-method (Knife-edge Equivalent Contact method), in which the rails, that are considered infinitely narrow, contact an equivalent wheel profile producing the same wheelset relative-track kinematics than using real wheel-rail profiles with a great computational efficiency.

On the other hand, the search of the contact points can be done using the so-called *offline* method. In this approach, the contact solution is solved in a preprocessing stage as a function of the wheelset relative position with respect to the track, and it is stored in a lookup table, that is

later used during the dynamic simulations by the interpolation in the stored data. In this sense, there are also many references that can be found in the literature about contact lookup tables [19, 20, 21, 22, 23, 24, 25, 26]. They can be related to both constraint or elastic approaches, although they are more suitable for the constraint one, since this formulation involves a reduced number of wheelset degrees of freedom (DOF) with respect to the track, as shown in [18]. This reduces the number of entries, and in turn the stored data, of the lookup tables. In [19], a constraint contact lookup table approach that accounts for track irregularities using two independent variables (2-DOFs) is proposed and compared with the online solution of the contact constraints. It is demonstrated that dealing carefully with geometric assumptions, simplified contact lookup tables produce accurate and efficient results. In [21], a 3-DOFs elastic contact lookup table is presented to study the advantages and disadvantages against an online procedure. The results showed that the time required for the lookup table approach is substantially lower than the online solution procedure. In [22], a combination of a constraint contact lookup table for the tread contact and an elastic online approach for the flange one is proposed and called *hybrid* method. It is extended in [23] to the combination of nodal and non-conformal contact detection, to solve significant jumps of contact points in turnouts. Moreover, in [24], a regularisation of the non-elliptical wheel-rail contact areas named Kalker book of tables for non-Hertzian contact (KBTNH) is proposed and used in [25, 26] to analyse accuracy and contact patch moments.

This paper focuses and supports the use of the constraint approach in some applications. Clearly, the elastic approach is better suited for a more detailed contact analysis, because it allows more insight into the actual surface areas in contact. However, under some common circumstances, the use of the constraint approach is superior:

1. When the profiles geometry is not well-known, due to wear for example.
2. When the overall vehicle dynamics is of interest, instead of the intimate wheel-rail contact analysis.

In addition, as it is accepted in the community, the constraint approach is computationally more efficient. However, one of its main drawbacks is its difficult application when dealing with two-point contact scenario. This scenario is very important in curving and safety analysis of the railway vehicles. That is why this paper focuses on this scenario.

To this end, this paper compares accuracy, efficiency, applicability and limitations of two constraint-based formulations (offline and online respectively) for the dynamic simulation of the wheel-rail contact of railway vehicles in multibody dynamics. The offline methodology used in this paper is based on precalculated contact lookup tables and the online one is based on the Knife-Edge equivalent Contact method (KEC-method) presented in [18]. The use of precalculated contact lookup tables is presented first. This method is well-known, computationally efficient and widely used. It is also presented an innovative procedure to interpolate between the stored data. However, an important drawback of lookup tables appears when using wheel-rail profile combinations that show two-point contact scenarios (tread contact and flange contact) because constraint contact lookup tables are not suitable to deal with simultaneous contacts using variable number of kinematic constraints. Since most of real wheel-rail profile combinations are of this type, this scenario is essential when analysing vehicle curving or wheel climbing and derailment. Instead, the two-point contact simulation with contact lookup tables is done in this work using a hybrid method in which the flange contact is analysed using a penetration-based elastic model. The second method used

in this paper is the KEC-method [18]. It is an online constraint-based method that considers the rails as infinitely narrow lines (like the edge of a knife) that contact equivalent wheels such that they show the same subspace of allowable motion that the real wheel and rail profiles. As it is a constraint-based method, the two-point contact scenario used together with a regularisation method for the tread-flange transition as presented in [27], allows possible wheel climbing.

The organisation of this paper is given as follows: Section 2 introduces the kinematics of the wheel-rail contact. Wheel-rail contact simulation with lookup tables and its interpolation procedure are presented in Section 3. The KEC-method approach is briefly explained in Section 4. Section 5 presents the generation of lookup tables for flanging wheelsets and Section 6 presents three case studies of a bogie vehicle to analyse differences and limitations of both approaches: (1) simulation results in a tangent-curved track with irregularities using profiles that do not show 2-point contacts, (2) simulation results in a tangent-curved track with irregularities using profiles that show 2-point contacts and (3) simulation results of a wheel climbing scenario in a small radius curved track without irregularities. Finally, Section 7 introduces an Author's comment about the selection of flange contact stiffness and Section 8 provides a summary and conclusion.

2. Kinematics of the wheel-rail contact

2.1. Track kinematics

Track geometry is the superposition of the ideal geometry and the irregularities. The components of the absolute position vector of an arbitrary point on the ideal track centreline with respect to a global frame is a function of the arc-length s, as follows:

$$\mathbf{R}^t(s) = \begin{bmatrix} R_x^t(s) \\ R_y^t(s) \\ R_z^t(s) \end{bmatrix}, \tag{1}$$

where $\mathbf{R}^t(s)$ contains the components of vector $\overrightarrow{R}^t$ shown in Fig. 1. The geometry of the track centreline 3D-curve is defined by the *horizontal profile* and the *vertical profile*. The so-called track preprocessors implement these functions of s given the ideal track geometry using a set of segment-dependent parameters (length, curvature, slope, etc.)

Fig. 1 shows the track frame $\langle O^t; X^t, Y^t, Z^t \rangle$ associated with the track centreline at each value of s. The orientation of the track frame with respect to a global frame can be measured with the Euler angles ψ^t (*azimut* or *heading* angle), θ^t (vertical slope, positive when downwards in the forward direction) and φ^t (*cant* or *superelevation* angle). These three angles are also functions of s that are implemented in the track pre-processor. The rotation matrix from the track frame to the global frame is given by:

$$\mathbf{A}^t(s) = \begin{bmatrix} \mathrm{c}\theta^t\mathrm{c}\psi^t & \mathrm{s}\varphi^t\mathrm{s}\theta^t\mathrm{c}\psi^t - \mathrm{c}\varphi^t\mathrm{s}\psi^t & \mathrm{s}\varphi^t\mathrm{s}\psi^t + \mathrm{c}\varphi^t\mathrm{s}\theta^t\mathrm{c}\psi^t \\ \mathrm{c}\theta^t\mathrm{s}\psi^t & \mathrm{c}\varphi^t\mathrm{c}\psi^t + \mathrm{s}\varphi^t\mathrm{s}\theta^t\mathrm{s}\psi^t & \mathrm{c}\varphi^t\mathrm{s}\theta^t\mathrm{s}\psi^t - \mathrm{s}\varphi^t\mathrm{c}\psi^t \\ -\mathrm{s}\theta^t & \mathrm{s}\varphi^t\mathrm{c}\theta^t & \mathrm{c}\varphi^t\mathrm{c}\theta^t \end{bmatrix}. \tag{2}$$

where the terms c and s in Eq. 2 refer to the cosine and sine functions respectively.

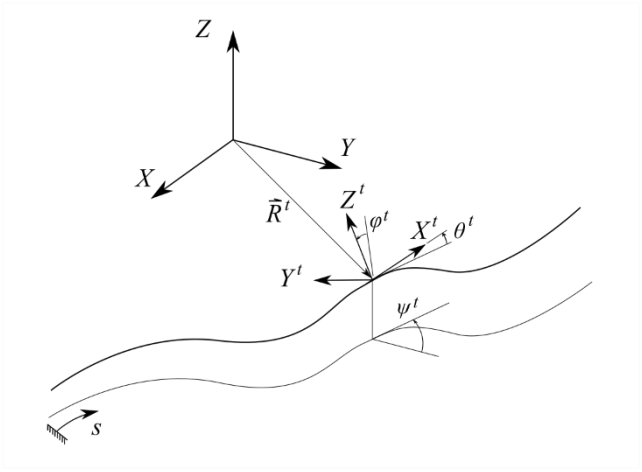

Fig. 1: Ideal track centreline

Fig. 2 on the left shows the relative position of the irregular right rail centreline with respect to the track frame. Fig. 2 on the right shows the displacement of the railheads due to irregularity in a cross-section of the track ($Y^t - Z^t$ plane). As observed in the figure, a frame is defined at each railhead (lrp, *left rail profile* frame, and rrp, *right rail profile* frame). Left and right rail profile frames are separated a distance $2L_r$ in the ideal track. The irregularity vectors $\overrightarrow{r}^{lir}$ (lir, *left rail irregularity*) and $\overrightarrow{r}^{rir}$ (rir, *right rail irregularity*) describe the displacement of the rail centrelines. The components of these vectors in the track frame are functions of s, given by:

$$\bar{\mathbf{r}}^{lir}(s) = \begin{bmatrix} 0 \\ y^{lir} \\ z^{lir} \end{bmatrix}, \qquad \bar{\mathbf{r}}^{rir}(s) = \begin{bmatrix} 0 \\ y^{rir} \\ z^{rir} \end{bmatrix} \tag{3}$$

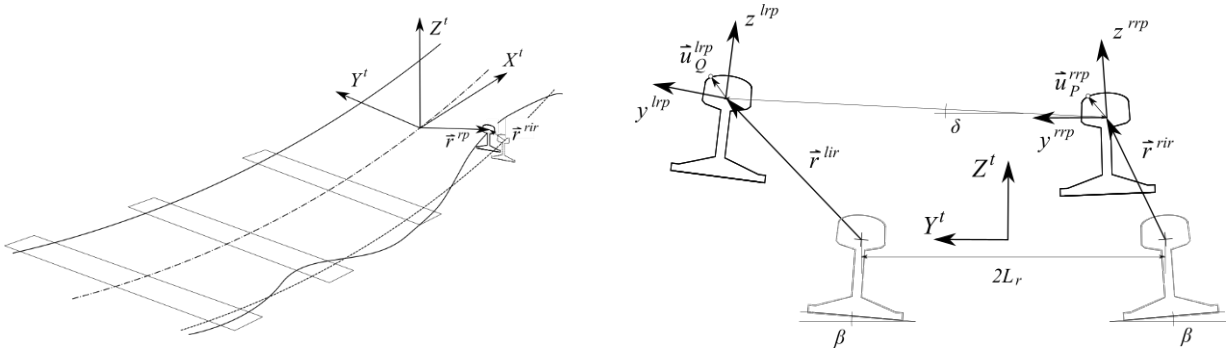

Fig. 2: Track irregularity

In the railway industry, the following four combinations of the railhead centrelines irregularities are measured:

- Alignment(al) : $al = (y^{lir} + y^{rir})/2$
- Verticle profile(vp) : $vp = (z^{lir} + z^{rir})/2$

- Gauge variation(gv) : $gv = y^{lir} - y^{rir}$
- Cross level(cl) : $cl = z^{lir} - z^{rir}$

The orientation of the railhead frames with respect to the track frame is given by the following rotation matrices:

$$\mathbf{A}^{t,lrp}(s) = \begin{bmatrix} 1 & 0 & 0 \\ 0 & \cos(\beta+\delta) & -\sin(\beta+\delta) \\ 0 & \sin(\beta+\delta) & \cos(\beta+\delta) \end{bmatrix}, \quad \mathbf{A}^{t,rrp}(s) = \begin{bmatrix} 1 & 0 & 0 \\ 0 & \cos(-\beta+\delta) & -\sin(-\beta+\delta) \\ 0 & \sin(-\beta+\delta) & \cos(-\beta+\delta) \end{bmatrix}, \tag{4}$$

where β is the orientation angle of the rail profiles and $\delta = (z^{lir} - z^{rir})/2L_r$ is the linearized rotation angle due to the irregularity. Both angles can be observed in Fig. 2 on the right.

The absolute position vectors of two points, P and Q, defined in the right and left railheads, respectively, are given by:

$$\begin{aligned} \overrightarrow{R}_P^{rrp} &= \overrightarrow{R}^t + \overrightarrow{r}^{rrp} + \overrightarrow{r}^{rir} + \overrightarrow{u}_P^{rrp}. \\ \overrightarrow{R}_Q^{lrp} &= \overrightarrow{R}^t + \overrightarrow{r}^{lrp} + \overrightarrow{r}^{lir} + \overrightarrow{u}_Q^{lrp}. \end{aligned} \tag{5}$$

The components of these vectors in the global frame are given by:

$$\begin{aligned} \mathbf{R}_P^{rrp} &= \mathbf{R}^t + \mathbf{A}^t(\bar{\mathbf{r}}^{rrp} + \bar{\mathbf{r}}^{rir} + \mathbf{A}^{t,rrp}\hat{\mathbf{u}}_P^{rrp}), \\ \mathbf{R}_Q^{lrp} &= \mathbf{R}^t + \mathbf{A}^t(\bar{\mathbf{r}}^{lrp} + \bar{\mathbf{r}}^{lir} + \mathbf{A}^{t,lrp}\hat{\mathbf{u}}_Q^{lrp}), \end{aligned} \tag{6}$$

where $\hat{\mathbf{u}}_P^{rrp}$ and $\hat{\mathbf{u}}_Q^{lrp}$ contain the components of the position vector of points P and Q in the rail profiles as shown in Fig. 2 on the right. These vectors are parametrized following the railhead profile geometry:

$$\hat{\mathbf{u}}_P^{rrp} = \begin{bmatrix} 0 \\ s_2^{rr} \\ h^r(s_2^{rr}) \end{bmatrix}, \qquad \hat{\mathbf{u}}_Q^{lrp} = \begin{bmatrix} 0 \\ s_2^{lr} \\ h^r(s_2^{lr}) \end{bmatrix}, \tag{7}$$

where lr and rr stand for *left rail* and *right rail*, s_2^{lr} and s_2^{rr} are the transverse coordinates of the points in the railheads and h^r is the function that defines the railhead profile, as shown in Fig. 3.

2.2. Vehicle kinematics

For the modelling of the railway vehicle, a set of relative body-track frame coordinates, as shown in Fig. 4, is selected in this work.

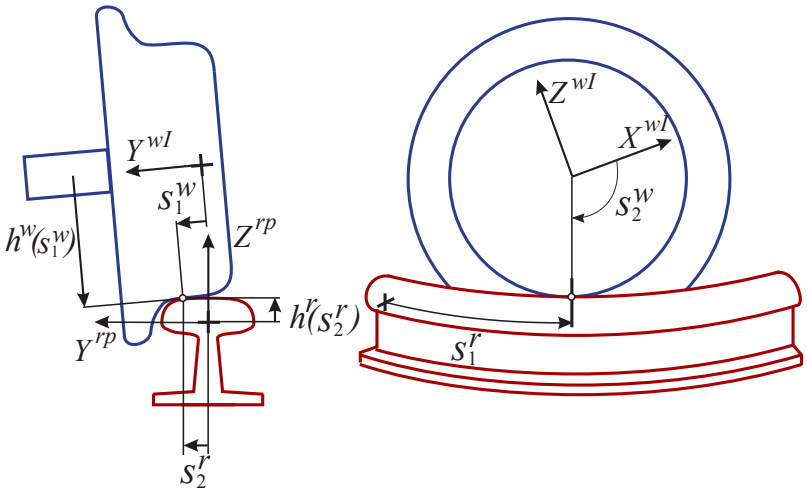

Fig. 3: Wheel profile and rail profile geometry

In this formulation, each modelled body belonging to the railway vehicle is accompanied by a track-frame along the track centreline. These frames are called *body-track frames* $\langle O^{bti}; X^{bti}, Y^{bti}, Z^{bti}\rangle$ for each body i. The body-track frame is defined such that the relative position vector $\bar{\mathbf{r}}^i = \begin{bmatrix} 0 & \bar{r}_y^i & \bar{r}_z^i \end{bmatrix}^T$ of the body frame with respect to the body-track frame has zero x component along the track centreline. Therefore, for each body i, the following set of coordinates:

$$\mathbf{q}^i = \begin{bmatrix} s^i & \bar{r}_y^i & \bar{r}_z^i & (\bar{\mathbf{\Phi}}^i)^T \end{bmatrix}^T = \begin{bmatrix} s^i & \bar{r}_y^i & \bar{r}_z^i & \bar{\varphi}^i & \bar{\theta}^i & \bar{\psi}^i \end{bmatrix}^T, \tag{8}$$

describe the absolute position of the body track frame (arc-length coordinate s^i), the relative body frame to body-track frame position (position vector $\bar{\mathbf{r}}^i$) and relative body frame to body-track frame orientation (orientation coordinates $\bar{\mathbf{\Phi}}^i$). Therefore, the set of coordinates for all vehicle bodies is:

$$\mathbf{q} = \begin{bmatrix} \mathbf{q}^2 \\ \vdots \\ \mathbf{q}^{nb} \end{bmatrix}, \tag{9}$$

where nb is the number of modelled bodies in the railway vehicle. Using these coordinates, the absolute position vector of point P that belongs to body i is given by:

$$\overrightarrow{R}_P^i = \overrightarrow{R}^{bti} + \overrightarrow{r}^i + \overrightarrow{u}_P^i. \tag{10}$$

where $\overrightarrow{R}_P^i$ (not shown in Fig. 1) is the absolute position vector of P, $\overrightarrow{R}^{bti}$ is the absolute position vector of the body-track frame, $\overrightarrow{r}^i$ is the relative position vector of the origin of the body i frame with respect to its body-track frame and $\overrightarrow{u}_P^i$ is the local position vector of point P in body i.

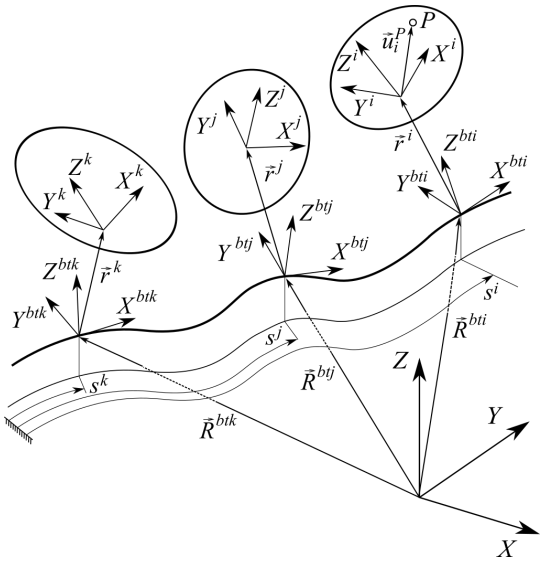

Fig. 4: Kinematics of the bodies of a railway vehicle with relative body-track frame coordinates

Eq. (10) can be projected in the global frame as follows:

$$\mathbf{R}_P^i = \mathbf{R}^{bti} + \mathbf{A}^{bti}(\bar{\mathbf{r}}^i + \mathbf{A}^{bti,i}\hat{\mathbf{u}}_P^i). \tag{11}$$

In this formula, the terms have the following meaning and functional dependency:

$\mathbf{R}^{bti} = \mathbf{R}^{bti}(s^i)$	Components of position vector of the body-track frame in the global frame.
$\mathbf{A}^{bti} = \mathbf{A}^{bti}(s^i)$	Transformation matrix of the body-track frame to the global frame.
$\bar{\mathbf{r}}^i = \bar{\mathbf{r}}^i(\mathbf{q})$	Components of position vector of the body with respect to the body-track frame in the body-track frame.
$\mathbf{A}^{bti,i} = \mathbf{A}^{bti,i}(\mathbf{q})$	Transformation matrix of the base body frame with respect to the body-track frame.
$\hat{\mathbf{u}}_P^i$	Components of the position vector of point P with respect to body i in the body frame. These components are constant.

2.3. Wheelset kinematics

For rigid wheelsets, it is convenient to introduce a new frame that is not used in any other vehicle body: the *wheelset intermediate frame*. The track-relative coordinates of the rigid wheelset i are:

$$\mathbf{q}^{wi} = \begin{bmatrix} s^{wi} & \bar{r}_y^{wi} & \bar{r}_z^{wi} & \bar{\varphi}^{wi} & \bar{\theta}^{wi} & \bar{\psi}^{wi} \end{bmatrix}^T. \tag{12}$$

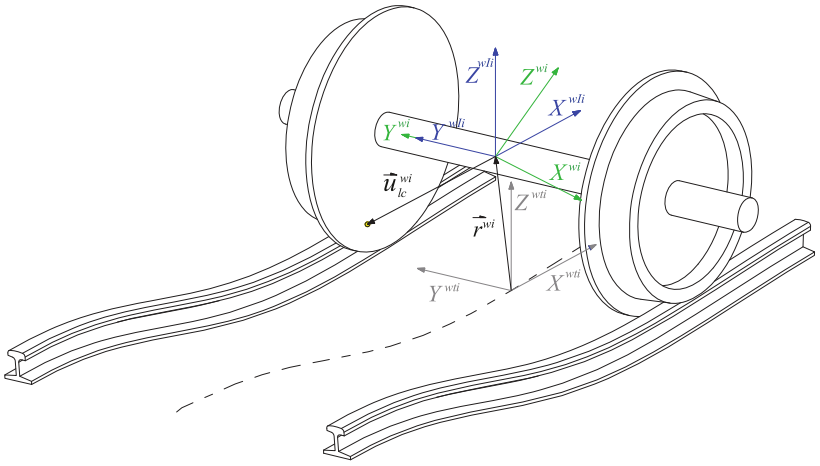

Fig. 5: Frames for rigid wheelset kinematics

It is convenient to define an additional frame for each wheelset, the intermediate wheelset frame, wIi, that rotates with the wheelset with the exception of the rolling angle $\bar{\theta}^{wi}$. Fig. 5 shows the wheelset i body frame wi and the intermediate one wIi. The orientation of the wheelset body frame with respect to the wheelset track frame wti is given by the following matrix:

$$\mathbf{A}^{wti,wi} = \mathbf{A}^{wti,wIi}(\bar{\psi}^{wi}, \bar{\varphi}^{wi})\mathbf{A}^{wIi,wi}(\bar{\theta}^{wi}), \tag{13}$$

where the brackets mean the functional dependency of the rotation matrices.

The use of the wheelset intermediate frame is convenient to describe the position of the wheel-rail contact points. This position varies very little in the wIi frame, but it greatly varies in the wi frame (this variation is approximately periodic, being the time taken by the wheel to complete a revolution the time-period). The position vector of a point P on the surface of the left or right wheel profile can be obtained as:

$$\mathbf{R}_P^{wi} = \mathbf{R}^{wti} + \mathbf{A}^{wti}(\bar{\mathbf{r}}^{wi} + \mathbf{A}^{wti,wIi}\hat{\mathbf{u}}_P^{wIi}), \tag{14}$$

where $\hat{\mathbf{u}}_P^{wIi}$ may take the following forms for the left ($P = L$) or right wheels ($P = R$):

$$\hat{\mathbf{u}}_R^{wIi} = \begin{bmatrix} h^{rw}(s_1^{rw})\cos s_2^{rw} \\ -L_w + s_1^{rw} \\ -h^{rw}(s_1^{rw})\sin s_2^{rw} \end{bmatrix}, \qquad \hat{\mathbf{u}}_L^{wIi} = \begin{bmatrix} h^{lw}(s_1^{lw})\cos s_2^{lw} \\ L_w + s_1^{lw} \\ -h^{lw}(s_1^{lw})\sin s_2^{lw} \end{bmatrix}, \tag{15}$$

where lw and rw stand for *left wheel* and *right wheel*, s_1^{lw}, s_2^{lw}, s_1^{rw} and s_2^{rw} are the parameters needed to the define the points in the wheel surface, h^{lw} and h^{rw} are the functions that defines the left and right wheel profile, as shown in Fig. 3 and L_w is the lateral distance of the wheel frames with respect to the wheelset frame.

2.4. Wheel-rail contact constraints

The wheel-rail non-conformal contact constraints (see Fig. 6) establish that the absolute position of the contact point on the rail is the same as the absolute position of the contact point on the wheel. In addition, the tangent plane to the rail at the contact point is parallel to the tangent plane to the wheel at the contact point. These are five constraint equations that can written as:

$$\begin{aligned}
&\mathbf{R}_c^{wi}(\mathbf{q}^{wi}, \mathbf{s}^w) - \mathbf{R}_c^{rp}(\mathbf{s}^r) = \mathbf{0}, \\
&\left[\mathbf{t}_{1,c}^{wi}(\mathbf{q}^{wi}, \mathbf{s}^w)\right]^T \mathbf{n}_c^{rp}(\mathbf{s}^r) = 0, \\
&\left[\mathbf{t}_{2,c}^{wi}(\mathbf{q}^{wi}, \mathbf{s}^w)\right]^T \mathbf{n}_c^{rp}(\mathbf{s}^r) = 0,
\end{aligned} \tag{16}$$

where c can be lc (left contact) or rc (right contact), w can be lw (left wheel) or rw (right wheel), rp can be lrp (left rail profile) or rrp (right rail profile), $\mathbf{s}^w = \begin{bmatrix} s_1^w & s_2^w \end{bmatrix}^T$, $\mathbf{s}^r = \begin{bmatrix} s_1^r & s_2^r \end{bmatrix}^T$ include all surface parameters needed to locate the contact points, $\mathbf{t}_{1,c}^{wi}$ and $\mathbf{t}_{2,c}^{wi}$ are the two unit-tangent vectors to the wheel surface at the contact point and $\mathbf{n}_c^{rp}$ is the normal vector to the rail surface at the contact point.

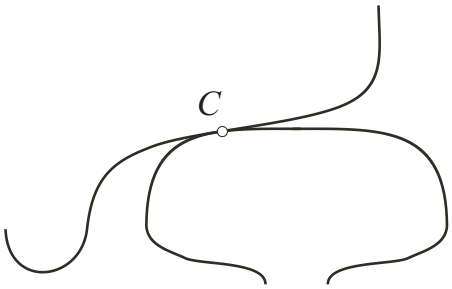

Fig. 6: Wheel and rail in contact

The approximate contact constraints represent a simplified version to Eq. (16). The approximate contact constraints neglect the influence of the wheelset yaw angle in the contact geometry. In other words, the 3D surface-to-surface contact constraints are reduced to 2D curve-to-curve contact constraints. The approximate contact constraints can be written as a set of three constraint equations per wheel-rail pair as follows:

$$\begin{aligned}
&\bar{\mathbf{r}}_c^{wi}(\mathbf{q}^{wi}, s_1^w) - \bar{\mathbf{r}}_c^{rp}(s_2^r) = \mathbf{0}, \\
&\left[\bar{\mathbf{t}}_{1,c}^{wi}(\mathbf{q}^{wi}, s_1^w)\right]^T \bar{\mathbf{n}}_c^{rp}(s_2^r) = 0,
\end{aligned} \tag{17}$$

In these equations, vectors are projected to the Y-Z plane of the track frame. That way, the set of surface parameters is reduced from 4 to 2. Only transverse parameters s_1^w and s_2^r to the profiles are needed. For that reason, the simplified nomenclature $s^w = s_1^w$ and $s^r = s_2^r$ will be used. More details about the contact constraints can be found in [19].

3. Wheel-rail contact simulation with lookup tables

This section explains the use of contact lookup tables for the simulation of railway vehicles using relative body-track frame coordinates.

3.1. Calculation of lookup tables

Lookup tables are calculated in a preprocessing stage. To create a contact lookup table, a set of discrete numerical values is assigned to the lateral displacement of the wheelset y^{wi} in a range that will be discussed in Section 5. The position along the track s^{wi} , pitch angle θ^{wi} and yaw angle ψ^{wi} are assumed to be zero because these coordinates have no influence on the contact geometry. For each of these positions, 6 simplified contact constraints Eq. (17) (3 for left contact and 3 for right contact) are solved to find the values of 6 coordinates: the wheelset position and orientation coordinates z^{wi} and φ^{wi} and the surface parameters s^{lw}, s^{rw}, s^{lr} and s^{rr} needed to locate the contact points on the left and right wheel and rail surfaces. The contact lookup table can be interpreted as a set of tabulated functions of the form:

$$\begin{aligned} &z^{wi} = z_{clt}(y^{wi}), \quad \varphi^{wi} = \varphi_{clt}(y^{wi}), \\ &s^{lw} = s^{lw}_{clt}(y^{wi}), \quad s^{lr} = s^{lr}_{clt}(y^{wi}) \quad s^{rw} = s^{rw}_{clt}(y^{wi}), \quad s^{rr} = s^{rr}_{clt}(y^{wi}), \end{aligned} \tag{18}$$

where the subscript *clt* stands for 'contact lookup table'. The contact lookup table can be used in dynamic simulations to find the values of these six coordinates from the value of the lateral displacement. In order to deal with a track with irregularities, the contact lookup table has to be extended from 1 entry to 2 entries. The process of creation of the contact lookup table has to be repeated for a set of values of the gauge variation (gv) in a range that covers the extreme values of the gauge that appear in practical applications. This is, the contact lookup table is recalculated a number of times after approaching and separating the rails from the nominal distance $2L_r$ shown in Fig. 2. That way, the functions given above become functions of two variables, as follows:

$$\begin{aligned} &z^{wi} = z_{clt}(y^{wi}, gv), \quad \varphi^{wi} = \varphi_{clt}(y^{wi}, gv) \\ &s^{lw} = s^{lw}_{clt}(y^{wi}, gv), \quad s^{lr} = s^{lr}_{clt}(y^{wi}, gv) \quad s^{rw} = s^{rw}_{clt}(y^{wi}, gv), \quad s^{rr} = s^{rr}_{clt}(y^{wi}, gv) \end{aligned} \tag{19}$$

The use of the lookup tables with irregular track is slightly different. In a dynamic simulation, given the longitudinal position of the wheelset s^{wi} , the values of the irregularities al, vp, gv and cl can be obtained. The lateral displacement that has to be used to enter the lookup table is not y^{wi} that gives the lateral displacement with respect to the ideal track centreline, but $\bar{y}^{wi} = y^{wi} - al$, that gives the lateral displacement with respect to the irregular track centreline. In turn, the outputs of the lookup table $\bar{z}^{wi}$ and $\bar{\varphi}^{wi}$ have to be interpreted differently, being $\bar{z}^{wi} = z^{wi} + vp$ and $\bar{\varphi}^{wi} = \varphi^{wi} + cl/2L_r$. The kinematic constraints associated with wheelset wi finally yield:

$$\mathbf{C}^{clt,wi} = \begin{bmatrix} z^{wi} - vp - z_{clt}(\bar{y}^{wi} + al, gv) \\ \varphi^{wi} - cl/2L_r - \varphi_{clt}(\bar{y}^{wi} + al, gv) \end{bmatrix} = \mathbf{0}. \tag{20}$$

More details in railway multibody simulation using contact lookup tables can be found in [19].

3.2. Interpolation in the lookup tables

The use of contact lookup tables that include track irregularities requires a special treatment in the interpolation procedure. If the generalised wheelset lateral displacement $\bar{y}^{wi}$ with respect to the irregular track centreline is considered constant within the interpolation between tables with different track gauge, considerable errors can be obtained when the contact points lie in the vicinity of the two-point or flange contact scenario. This can be explained with the help of Fig. 7 (where superscript wi is omitted for simplicity).

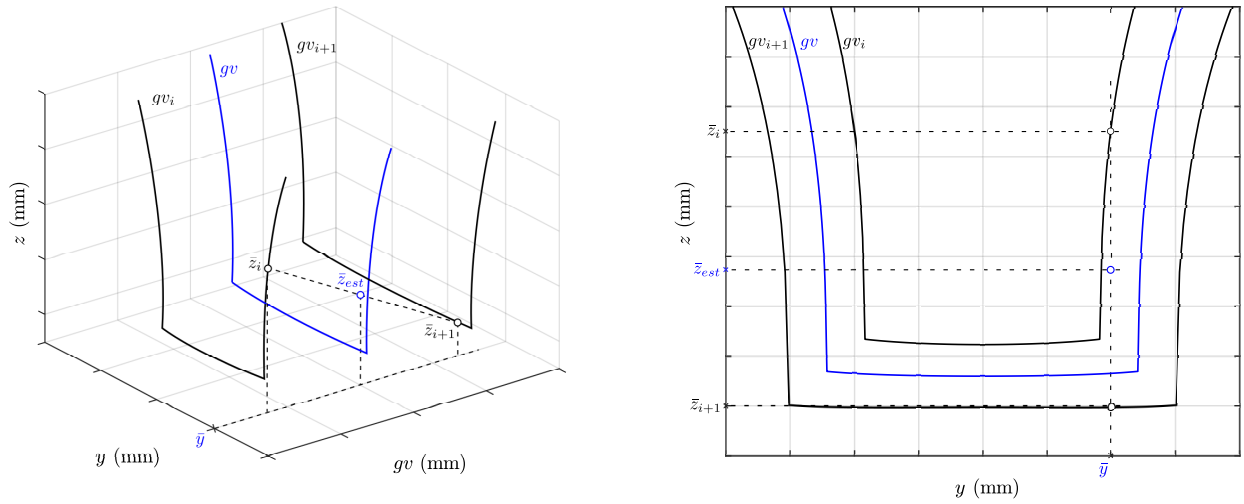

Fig. 7: Interpolation error at contact lookup tables with track irregularities

Fig. 7 shows in solid dark lines the wheelset vertical coordinate $\bar{z}^{wi}$ stored in the lookup table for two different values of gauge irregularity (gv_i and gv_{i+1}) and in solid blue line the same for an arbitrary track gauge irregularity gv between gv_i and gv_{i+1} that is not stored in the table. Let us assume that in a specific instant of a simulation with track gauge gv , the wheelset lateral displacement $\bar{y}^{wi}$ is in the vicinity of the two-point wheel-rail contact scenario such that in table gv_{i+1} with $\bar{y}^{wi}$ the wheelset is at a single point tread contact $\bar{z}^{wi}_{i+1}$, while in table gv_i the wheelset is at a wheel climb scenario $\bar{z}^{wi}$. Obviously, the interpolation between $\bar{z}^{wi}_i$ and $\bar{z}^{wi}_{i+1}$ provides an estimated wheelset vertical displacement $\bar{z}^{wi}_{est}$ that is far of the correct value given by the blue line.

In order to avoid these interpolation errors, the wheelset lateral displacement $\bar{y}^{wi}$ has to be updated to the values $\bar{y}^{wi}_i$ and $\bar{y}^{wi}_{i+1}$ that correspond to gauge variations gv_i and gv_{i+1} that are stored in the table. This procedure, which is shown in Fig. 8, is defined as follows:

- Given $\bar{y}^{wi}_i$ and gv , find the point of convergence O and its theoretical irregularity gv_O as:

$$gv_O = gv_{i+1} - \frac{\bar{y}^f_{i+1} \cdot (gv_{i+1} - gv_i)}{\bar{y}^f_{i+1} - \bar{y}^f_i} \tag{21}$$

  where superscript f refers to the flange starting point. Note that gv_O is a conceptual gauge irregularity in which both wheels experience flange contact and the wheelset has no possible lateral displacement.

- Interpolate in the direction $O - \bar{y}^{wi}$ to obtain the corresponding two lateral displacements $\bar{y}_i^{wi}$ and $\bar{y}_{i+1}^{wi}$.
- Enter the lookup tables gv_i and gv_{i+1} with $\bar{y}_i^{wi}$ and $\bar{y}_{i+1}^{wi}$ to obtain the contact solutions at the stored tables (i.e. $\bar{z}_i^{wi}$ and $\bar{z}_{i+1}^{wi}$ for the vertical displacement, $\bar{\varphi}_i^{wi}$ and $\bar{\varphi}_{i+1}^{wi}$ for the roll angle).
- Interpolate between the stored solutions to obtain the accurate coordinate (i.e. $\bar{z}_{est}^{wi}$ and $\bar{\varphi}_{est}^{wi}$).

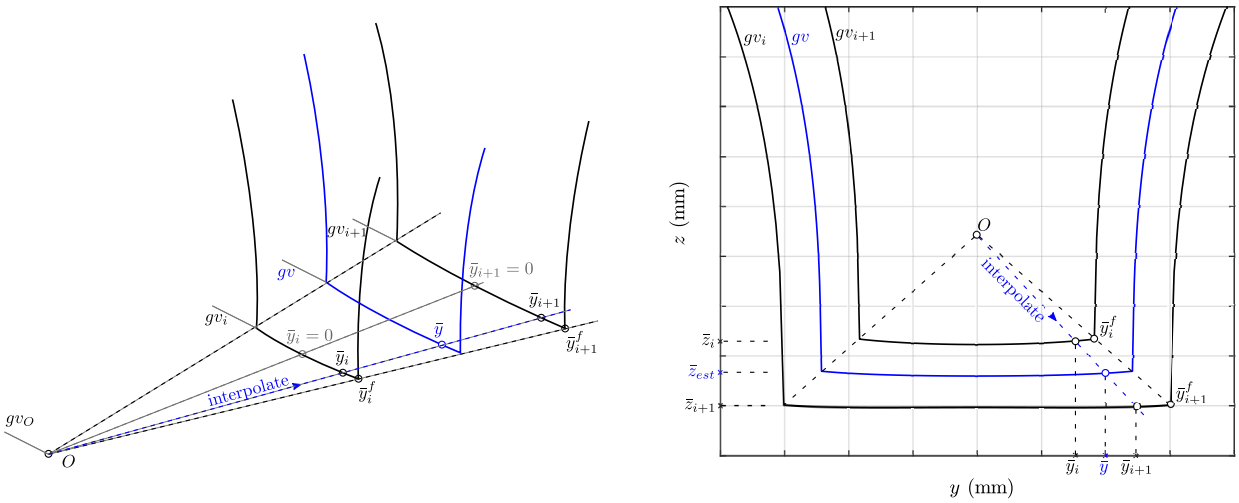

Fig. 8: Interpolation method at contact lookup tables with track irregularities

As it is shown by Fig. 7 and Fig. 8, the described interpolation procedure avoids errors that can be considerably high at the vicinity of the flange contact scenario.

3.3. Calculation of contact forces when using lookup tables

Contact forces are divided into normal contact forces and tangential contact forces. When using lookup tables, normal contact forces in the tread are computed as reaction forces associated with the contact constraints, while normal contact forces in the flange are computed as elastic forces as a function of the wheel-rail penetration. For both, tread and flange contact, tangential contact forces are computed as applied forces using any established creep contact theory (as Kalker non-linear theory [28] or Polach theory [29]). The resulting equations of motion of the railway vehicle yield:

$$\begin{bmatrix} \mathbf{M} & \left(\mathbf{C}_{\mathbf{q}}^{clt}\right)^T \\ \mathbf{C}_{\mathbf{q}}^{clt} & \mathbf{0} \end{bmatrix} \begin{bmatrix} \ddot{\mathbf{q}} \\ \boldsymbol{\lambda} \end{bmatrix} = \begin{bmatrix} \mathbf{Q} + \mathbf{Q}_{fla}^{nor} + \mathbf{Q}^{tang} \\ -\dot{\mathbf{C}}_{\mathbf{q}}^{clu} \dot{\mathbf{q}} \end{bmatrix} \tag{22}$$

where $\mathbf{M}$ is the vehicle mass matrix, $\mathbf{C}_{\mathbf{q}}^{clt}$ is the Jacobian matrix of all wheel-rail contact constraints modelled with lookup tables, $\boldsymbol{\lambda}$ is the array of Lagrange multipliers, $\mathbf{Q}_{fla}^{nor}$ is the vector of generalised wheel-rail normal flange forces, $\mathbf{Q}^{tang}$ is the vector of generalised tangential tread and flange forces, and $\mathbf{Q}$ include all other generalised applied forces and generalised quadratic-velocity inertia forces. For clarity, in this equation it has been assumed that the only constraints in the vehicle system

are those due to the wheel rail contact. However, everything is valid under the existence of other constraints.

The generalised normal forces at the wheel tread are computed using the Lagrange multipliers technique. Therefore, these forces are treated as reaction forces whose value can be computed as:

$$\mathbf{Q}^{nor}_{tread} = -\left(\mathbf{C}^{clt}_{\mathbf{q}}\right)^T \boldsymbol{\lambda}. \tag{23}$$

The Jacobian matrix $\mathbf{C}^{clt}_{\mathbf{q}}$ is an assembly of the Jacobian matrices $\mathbf{C}^{clt,wi}_{\mathbf{q}}$ associated with each wheelset, that is given by:

$$\mathbf{C}^{clt,wi}_{\mathbf{q}} = \begin{bmatrix} -\frac{\mathrm{d}vp}{\mathrm{d}s^{wi}} - \frac{\partial z_{clt}}{\partial y}\frac{\mathrm{d}al}{\mathrm{d}s^{wi}} - \frac{\partial z_{clt}}{\partial gv}\frac{\mathrm{d}gv}{\mathrm{d}s^{wi}} & -\frac{\partial z_{clt}}{\partial y} & 1 & 0 & 0 & 0 \\ -\frac{1}{2L_r}\frac{\mathrm{d}cl}{\mathrm{d}s^{wi}} - \frac{\partial \varphi_{clt}}{\partial y}\frac{\mathrm{d}al}{\mathrm{d}s^{wi}} - \frac{\partial \varphi_{clt}}{\partial gv}\frac{\mathrm{d}gv}{\mathrm{d}s^{wi}} & -\frac{\partial \varphi_{clt}}{\partial y} & 0 & 1 & 0 & 0 \end{bmatrix} \tag{24}$$

In this matrix the fact that the irregularities al, vp, gv and cl are a functions of the wheelset position along the track s^{wi}, has been accounted for. However, because these function use to be such that the derivatives with respect to s^{wi} are very small, the Jacobian matrix can be simplified to:

$$\mathbf{C}^{clt,wi}_{\mathbf{q}} = \begin{bmatrix} 0 & -\frac{\partial z_{clt}}{\partial y} & 1 & 0 & 0 & 0 \\ 0 & -\frac{\partial \varphi_{clt}}{\partial y} & 0 & 1 & 0 & 0 \end{bmatrix} \tag{25}$$

The generalised normal forces at the wheel flange are treated as applied forces. In this research, the flange force at wheelset i (wi) is computed as:

$$\begin{aligned} \mathbf{Q}^{nor,wi}_{fla} &= \left(\frac{\partial \bar{\mathbf{r}}^{wi}_{fla}}{\partial \mathbf{q}^{wi}}\right)^T \mathbf{F}^{nor,wi}_{fla}, \\ \mathbf{F}^{nor,wi}_{fla} &= \begin{cases} K_{hertz}(\delta^{wi})^{3/2} + C_{damp}\dot{\delta}^{wi}|\delta^{wi}| & \text{if} \quad \delta^{wi} > 0 \\ \mathbf{0} & \text{if} \quad \delta^{wi} \leq 0 \end{cases}, \end{aligned} \tag{26}$$

where $\bar{\mathbf{r}}^{wi}_{fla}$ is the position vector of the contact point in the flange, $\mathbf{F}^{nor,wi}_{fla}$ is the elastic normal force in the flange, δ^{wi} is the wheel-rail penetration at the flange contact, K_{hertz} is the Hertzian stiffness and C_{damp} is a constant that introduces non-linear damping. Note that the terms $\bar{\mathbf{r}}^{wi}_{fla}$, δ^{wi} and K_{hertz} are interpolated from the lookup table.

For the calculation of the contact-tangential creep forces that result in $\mathbf{Q}^{tang}$ the following data are needed for each wheel-rail contact point (either tread or flange contact):

1. The normal contact force.
2. The relative velocity of the contact points

3. Kalker's constants and coefficient of friction

Here two problems arise just for the tread contacts:

1. The generalised normal forces $\mathbf{Q}^{nor}_{tread}$ (reaction forces) are known only after solving Eq. (20) and
2. The calculation of the normal force at wheelset wi, $\mathbf{F}^{nor,wi}_{tread}$, from the generalised elastic force $\mathbf{Q}^{nor}_{tread}$ is not straight forward.

The solution to the first problem, that being strict would require an iterative solution of the equations of motion Eq. (22), is practically solved by assuming that the normal forces this time-step equal the normal forces obtained last time-step. This simple assumption works efficiently in practice. The second problem requires some more effort.

The vertical force $\bar{F}^{wi}_z$ (vertical component in the track frame) and roll torque $\hat{M}^{wi}_x$ (longitudinal component in the wheelset intermediate frame) at the wheelset due to the normal contact forces on the treads can be easily identified as the third and fourth component of $\mathbf{Q}^{nor,wi}_{tread}$, as follows:

$$\begin{aligned} \mathbf{Q}^{nor,wi}_{tread} &= -\left(\mathbf{C}^{clu,wi}_{\mathbf{q}}\right)^T \boldsymbol{\lambda}^{wi} \\ \bar{F}^{wi}_z = \mathbf{Q}^{nor,wi}_{tread}(3), &\quad \hat{M}^{wi}_x = \mathbf{Q}^{nor,wi}_{tread}(4). \end{aligned} \tag{27}$$

This is clear due to the physical interpretation of the reaction forces. These force and torque are due to the normal contact forces at the left tread $F^{nor,wi}_{ltread}$ and the right tread $F^{nor,wi}_{rtread}$ as shown by Fig. 9. The direction of these forces $\overrightarrow{n}_{ltread}$ and $\overrightarrow{n}_{rtread}$ are the normal vectors to the wheel surfaces that are stored in the lookup table since they only depend on the lateral displacement and the irregularity. A simple force and torque balance gives the following results:

$$\begin{aligned} &F^{nor,wi}_{ltread}\left(\bar{\mathbf{n}}_{ltread}\right)_z + F^{nor,wi}_{rtread}\left(\bar{\mathbf{n}}_{rtread}\right)_z = \bar{F}^{wi}_z \\ &F^{nor,wi}_{ltread}(\hat{\mathbf{r}}_{ltread} \times \hat{\mathbf{n}}_{ltread})_x + F^{nor,wi}_{rtread}(\hat{\mathbf{r}}_{rtread} \times \hat{\mathbf{n}}_{rtread})_x = \hat{M}^{wi}_x \end{aligned} \tag{28}$$

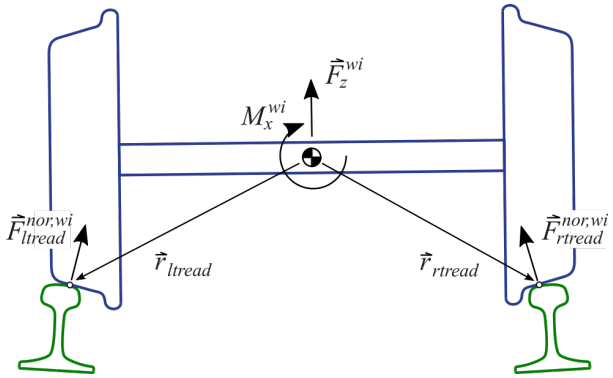

Fig. 9: Forces and torque on wheelset

This equation can be turn into a set of two linear algebraic equations that can be used to find the normal contact forces at the treads each time step. Input data are the reaction force and torque, that appear as an independent term, and the contact geometry (position of contact points and normal to the wheels at these points), that appear in the coefficient matrix and can be extracted from the contact lookup table, as follows:

$$\begin{bmatrix} \left(\bar{\mathbf{n}}_{ltread}\right)_z & \left(\bar{\mathbf{n}}_{rtread}\right)_z \\ (\hat{\mathbf{r}}_{ltread} \times \hat{\mathbf{n}}_{ltread})_x & (\hat{\mathbf{r}}_{rtread} \times \hat{\mathbf{n}}_{rtread})_x \end{bmatrix} \begin{bmatrix} F^{nor,wi}_{ltread} \\ F^{nor,wi}_{rtread} \end{bmatrix} = \begin{bmatrix} \bar{F}^{wi}_z \\ \hat{M}^{wi}_x \end{bmatrix} \tag{29}$$

Once the location of the contact points and the normal contact forces at the tread and the flange of the wheels are known, the generalised tangential forces $\mathbf{Q}^{tang}$ at these points can be computed. In this investigation, Polach method is used [29] because of its good balance between accuracy and simplicity. To this end, the relative velocity of the contact point on the wheels with respect to the contact point on the rails has to be calculated. These velocities are divided by the wheelset forward velocity to find the so-called creepages. Polach method uses the Kalker's linear coefficients. These coefficients depend on the material properties of the wheel and rail, the curvatures of the surfaces at the contact points and the normal contact force. The curvatures and the normal contact forces are used to find the semi-axis of the contact ellipse (Hertz theory is assumed to be valid). This calculation each time step at each wheelset consumes a lot of computational time. Kalker's linear coefficients cannot be precomputed because the value of the normal contact forces is not known in the pre-processing stage. The strategy followed in this research is to pre-compute the Kalker's linear coefficients for each wheel-rail contact geometry used in the lookup table for a normal contact force equal to one. These "unit-force Kalker's linear coefficients" are stored in the lookup table such that the calculation of the actual ones are very simply obtained online.

4. Wheel-rail contact simulation with KEC-equivalent profiles

This section presents the use of KEC-equivalent profiles for the simulation of railway vehicles using relative body-track frame coordinates.

4.1. KEC-equivalent profiles

The KEC-equivalent profile associated with the wheel-rail profiles combination has the property that, when contacting ideal railheads with zero width, results in a wheelset with the same space of allowable motion than the wheelset with the real wheel-rail profiles combination. All details about this method can be seen in [18, 27]. Fig. 10 on the left shows two wheelsets contacting rails. The sketch on the top with the real wheel-rail profiles combination while the sketch below with the KEC-equivalent profile. The subspace of allowable motion is characterised by the functions $z^{wi} = z_{clt}(y^{wi})$, $\varphi^{wi} = \varphi_{clt}(y^{wi})$, that are plot on the right-upper part of the figure. The real and KEC-equivalent wheel profiles are shown in the right-lower part of the figure.

The contact constraint equations of a wheelset with KEC-equivalent profiles has very simple form

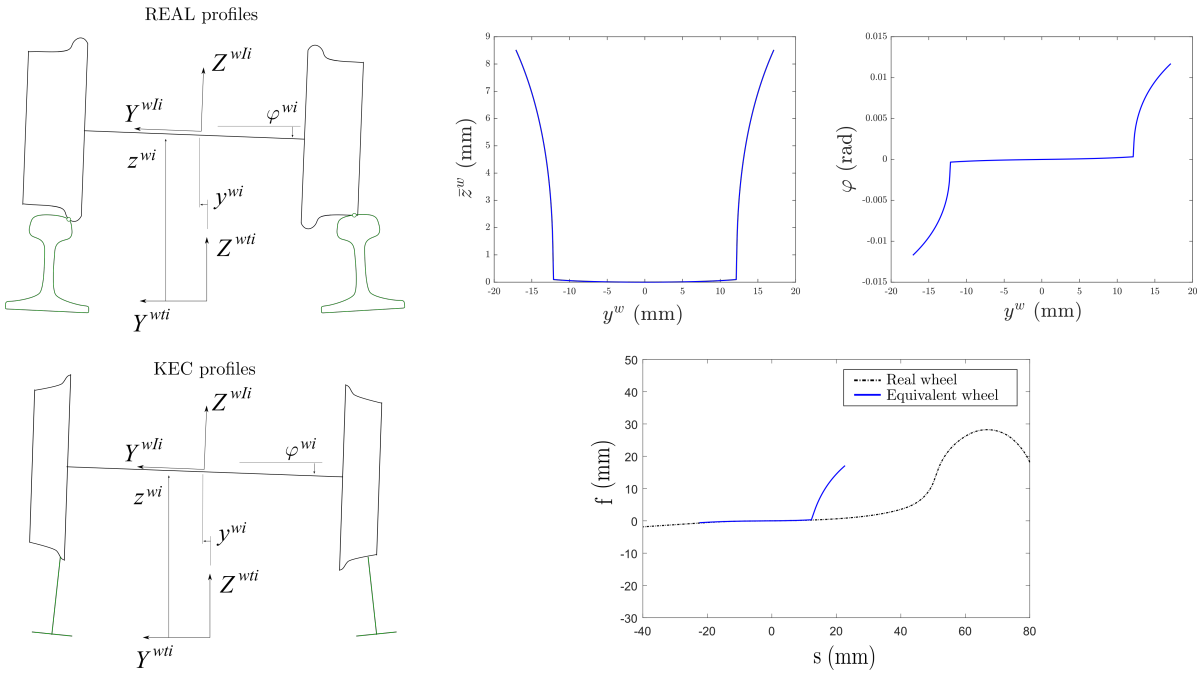

Fig. 10: Real profile and KEC equivalent wheel profile

compared with Eq. (17). These equations are given by:

$$\mathbf{C}^{KEC,wi}(\mathbf{q}^{wi},\mathbf{s}^k) = \begin{bmatrix} 0 & r_0+f^{lk} & 1 & 0 \\ 0 & r_0+f^{rk} & 0 & 1 \\ 1 & L_w & \varphi^{wi} & 0 \\ 1 & -L_w & 0 & \varphi^{wi} \end{bmatrix} \begin{bmatrix} \bar{z}^{wi} \\ \varphi^{wi} \\ s^{lk} \\ s^{rk} \end{bmatrix} - \begin{bmatrix} y^{wi}-y^{lir} \\ y^{wi}-y^{rir} \\ -f^{lk}-z^{lir} \\ -f^{rk}-z^{rir} \end{bmatrix} \tag{30}$$

where $\mathbf{s}^k = \begin{bmatrix} s^{lk} & s^{rk} \end{bmatrix}^T$ are the lateral positions of the contact point in the left and right KEC-equivalent profiles, f^{lk} and f^{rk} are the value of the equivalent profiles at these locations and r_0 is the rolling radius of the wheel when centered in the track. The main advantage of the use of KEC-equivalent profiles instead of the real ones are [18, 27]:

1. Contact forces on the tread and the flange are treated equally (avoiding hybrid methods).
2. Contact constraints can be solved online keeping a good computational efficiency.
3. Wheel climbing can be simulated.
4. Two-point contact scenario can be simulated with a smooth transition of the normal contact forces from tread to flange.

4.2. Equivalence of lookup tables and KEC-method in irregular tracks

In the KEC method, the computation of the equivalent wheel profiles requires the wheelset kinematics with respect to an ideal track [18]. However, these profiles can be used in irregular tracks with accuracy. This is an advantage with respect to traditional contact lookup tables that need to store the wheelset kinematics and contact solution for tracks with a set of different values of the gauge. This is, the lookup table contact method requires a 2-entry table, while the KEC-method requires a

1-entry table. Nonetheless, the resulting KEC profiles appear to be valid for different values of the gauge, as shown below.

To show this equivalence in irregular tracks, the wheelset kinematics using contact lookup tables and KEC-method is compared next. To that end, a wheelset with wheels S1002 profile and rails LB.140-AREA profile are considered [27]. Fig. 11 and Fig. 12 show the wheelset vertical displacement and roll angle coordinate with respect to the track centreline within a range of track gauge variations Δgv of ± 9 mm respectively.

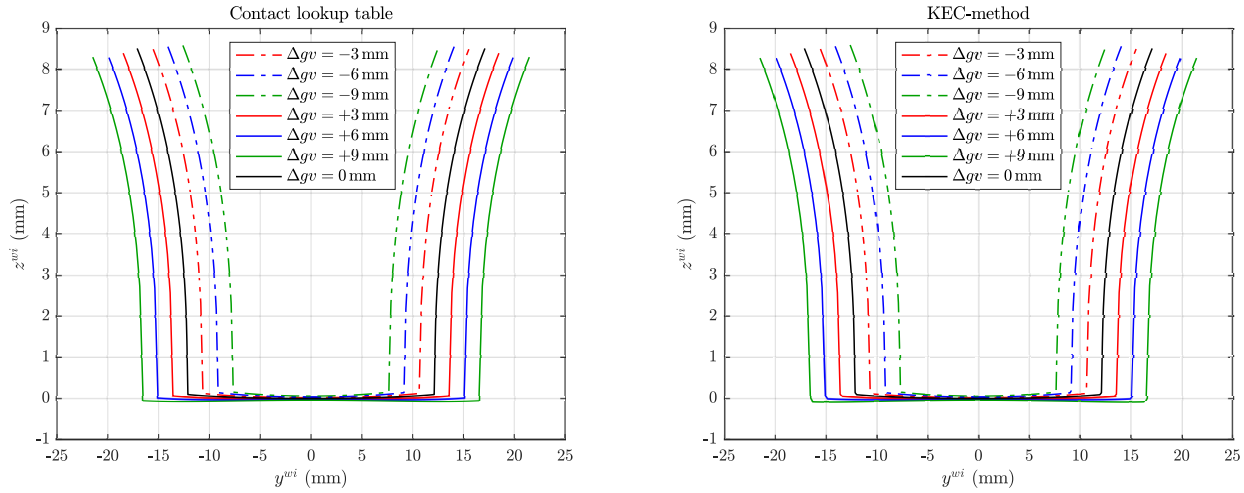

Fig. 11: Wheelset vertical displacement with respect to track centreline for different values of gauge irregularity. Left: contact lookup table. Right: KEC-method

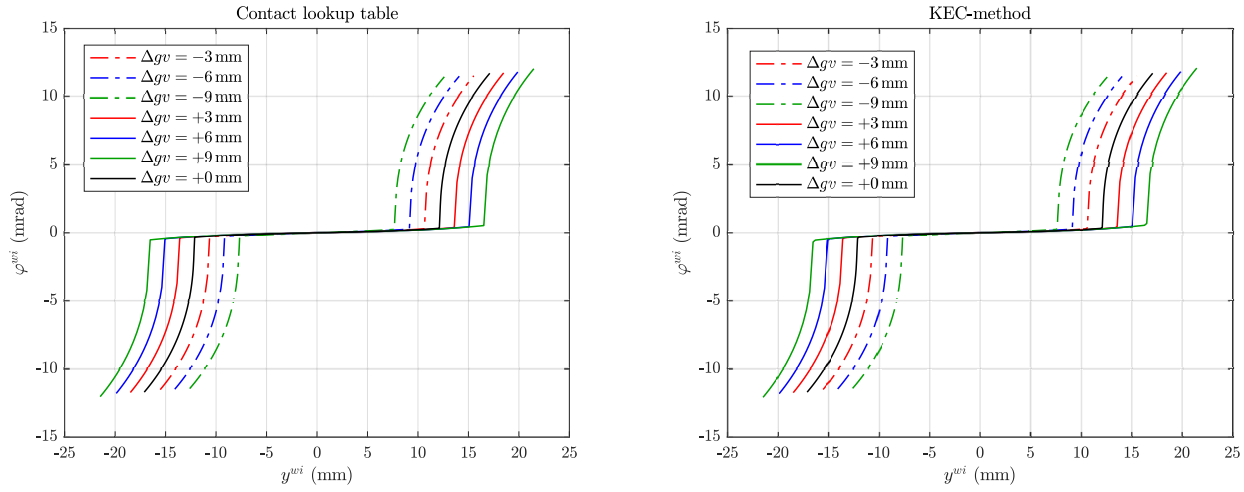

Fig. 12: Wheelset roll angle with respect to track centreline for different values of gauge irregularity. Left: contact lookup table. Right: KEC-method

Fig. 13 and Fig. 14 show the absolute differences between the contact solution using lookup tables and KEC-method. As shown in both figures, the error obtained for both wheelset vertical displacement and roll angle is bigger the higher the gauge variation is. This outermost case, which is given by a 9-mm track gauge variation, provides a 60 μm vertical distance and a 0.16 mrad errors when the

contact point is at the flange before wheel climb. These are quite low errors when compared to the high-order magnitudes given at Fig. 11 and Fig. 12 respectively. Moreover, those differences are almost inappreciable when the contact point lies on the tread. It can be concluded that the KEC-method provides an accurate kinematic solution for its use in tracks with irregularities.

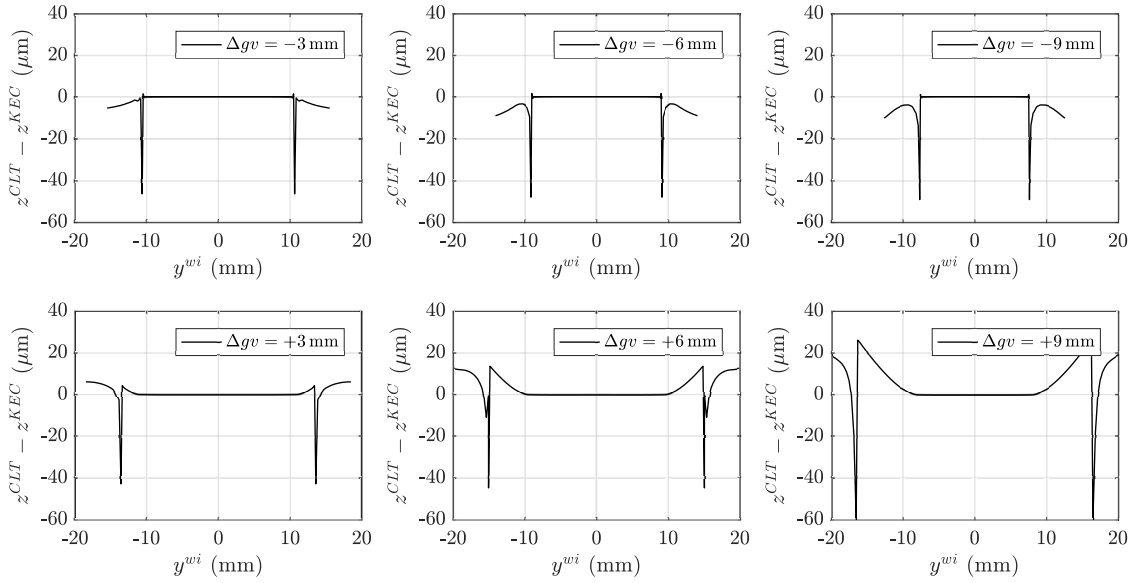

Fig. 13: Absolute differences in the wheelset vertical displacement with respect to track centreline for different values of gauge irregularity.

4.3. Calculation of contact forces when using the KEC method

When using the KEC method two main difficulties are found:

1. Normal contact forces cannot be obtained with the classical Lagrange multiplier method.
2. The tangential contact forces cannot be applied on the equivalent profile.

The second problem has an easy solution. When finding the KEC-equivalent profile, a table is created to find the position of the contact points in the real profiles once the position of the contact points in the KEC-equivalent profile is found solving Eq. (30). The solution of the first problem is more involved.

Eq. (30) is written in terms of the wheelset coordinates $\mathbf{q}^{wi}$ and the profile parameters $\mathbf{s}^k$. If these profile parameters could be eliminated from Eq. (30), reducing it to a set of two equations and three unknowns (y^{wi}, z^{wi} and φ^{wi}), just like Eq. (20), then the problem would be solved and the Lagrange multipliers method could be used to find the normal contact forces. Unfortunately, the elimination of $\mathbf{s}^k$ is not possible due to the non-linearity of Eq. (30). It can be concluded that, for the KEC-method:

$$\mathbf{Q}^{nor} \neq -\left(\mathbf{C}_{\mathbf{q}}^{KEC}\right)^T \boldsymbol{\lambda}. \tag{31}$$

where the Jacobian matrix $\mathbf{C}_{\mathbf{q}}^{KEC}$ is the result of assembling the Jacobian matrices $\mathbf{C}_{\mathbf{q}}^{KEC,wi}$ associated with all wheelsets in the vehicle.

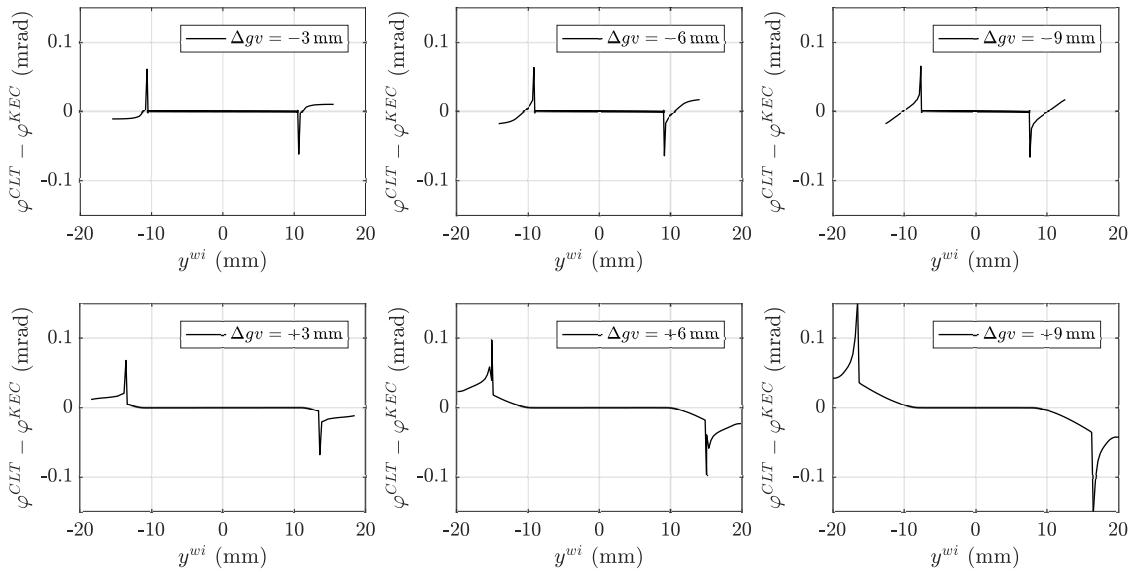

Fig. 14: Absolute differences in the wheelset roll angle with respect to track centreline for different values of gauge irregularity.

In the classical method of the Lagrange multipliers, the rows of the Jacobian matrix provide the direction of the reaction forces in the space of the generalised coordinates, while the multipliers mean the number that these rows have to be multiplied by to obtain the generalised reaction forces. In the problem at hand, the Jacobian matrix is not needed to find the direction of the reaction forces, because these directions are known in advance: the normal vectors to the real wheel profiles. Therefore, the reaction forces for wheelset wi can be obtained as:

$$\mathbf{Q}^{nor} = -\begin{bmatrix} \bar{\mathbf{n}}_{lw} & \bar{\mathbf{n}}_{rw} \\ \hat{\mathbf{r}}_{lw} \times \hat{\mathbf{n}}_{lw} & \hat{\mathbf{r}}_{rw} \times \hat{\mathbf{n}}_{rw} \end{bmatrix} \begin{bmatrix} \lambda_{lw}^{wi} \\ \lambda_{rw}^{wi} \end{bmatrix} = -\mathbf{N}^{wi}\boldsymbol{\lambda}^{wi} \tag{32}$$

The coefficient matrix $\mathbf{N}^{wi}$ of this equation looks similar to the one that appear in Eq. (29). However, $\mathbf{N}^{wi}$ includes the complete set vector components (it is 6×2) instead of single components (the one in Eq. (29) is 2×2). An important benefit of this alternative formulation of the Lagrange multipliers method is that the multipliers can be directly identified with the normal contact forces, this is:

$$\begin{aligned} F_{lw}^{nor,wi} &= \lambda_{lw}^{wi}, \\ F_{rw}^{nor,wi} &= \lambda_{rw}^{wi}. \end{aligned} \tag{33}$$

Therefore, once the Lagrange multipliers are obtained after solving the equations of motion each time-step, no additional equations, like Eq. (29), has to be solved to find the normal contact forces.

The equations of motion of the vehicle in DAE form, index 1, like Eq. (22), include the second time-derivative of the constraint equations. In these derivatives, the wheelset accelerations have to be isolated with respect to $\mathbf{s}^k$. In this case, this isolation has no difficulty because the constraint equations at acceleration level are linear. The process starts with the calculation of the first time-derivative of the KEC constraints, as follows:

$$\dot{\mathbf{C}}^{KEC,wi} = \frac{\partial \mathbf{C}^{KEC,wi}}{\partial \mathbf{q}^{wi}}\dot{\mathbf{q}}^{wi} + \frac{\partial \mathbf{C}^{KEC,wi}}{\partial \mathbf{s}^{k}}\dot{\mathbf{s}}^{k} + \begin{bmatrix} \dot{y}^{lir} \\ \dot{z}^{lir} \\ \dot{y}^{rir} \\ \dot{z}^{rir} \end{bmatrix} = \mathbf{C}_{\mathbf{q}}^{KEC,wi}\dot{\mathbf{q}}^{wi} + \mathbf{C}_{\mathbf{s}}^{KEC,wi}\dot{\mathbf{s}}^{k} + \dot{\mathbf{x}}^{ir} = \mathbf{0}, \quad (34)$$

where $\mathbf{x}^{ir}$ includes the four track irregularities. The second-time derivative of the constraints are given by:

$$\ddot{\mathbf{C}}^{KEC,wi} = \mathbf{C}_{\mathbf{q}}^{KEC,wi}\ddot{\mathbf{q}}^{wi} + \mathbf{C}_{\mathbf{s}}^{KEC,wi}\ddot{\mathbf{s}}^{k} + \dot{\mathbf{C}}_{\mathbf{q}}^{KEC,wi}\dot{\mathbf{q}}^{wi} + \dot{\mathbf{C}}_{\mathbf{s}}^{KEC,wi}\dot{\mathbf{s}}^{k} + \ddot{\mathbf{x}}^{ir} = \mathbf{0}. \quad (35)$$

The Jacobian matrices $\mathbf{C}_{\mathbf{q}}^{KEC,wi}$ (4×6) and $\mathbf{C}_{\mathbf{s}}^{KEC,wi}$ (4×2) can be separated into two submatrices with two rows each, as follows:

$$\mathbf{C}_{\mathbf{q}}^{KEC,wi} = \begin{bmatrix} \mathbf{C}_{\mathbf{q}}^{a} \\ \mathbf{C}_{\mathbf{q}}^{b} \end{bmatrix}, \quad \mathbf{C}_{\mathbf{s}}^{KEC,wi} = \begin{bmatrix} \mathbf{C}_{\mathbf{s}}^{a} \\ \mathbf{C}_{\mathbf{s}}^{b} \end{bmatrix}. \quad (36)$$

The two second equations of the second time-derivative of the constraints (Equations b) can be manipulated to isolate $\ddot{s}^k$, as follows:

$$\begin{aligned} &\mathbf{C}_{\mathbf{q}}^{b}\ddot{\mathbf{q}}^{wi} + \mathbf{C}_{\mathbf{s}}^{b}\ddot{\mathbf{s}}^{k} = -\dot{\mathbf{C}}_{\mathbf{q}}^{b}\dot{\mathbf{q}}^{wi} - \dot{\mathbf{C}}_{\mathbf{s}}^{b}\dot{\mathbf{s}}^{k} - (\ddot{\mathbf{x}}^{ir})^{b} \Rightarrow \\ &\Rightarrow \ddot{\mathbf{s}}^{k} = -(\mathbf{C}_{\mathbf{s}}^{b})^{-1}\Big[\mathbf{C}_{\mathbf{q}}^{b}\ddot{\mathbf{q}}^{wi} + \dot{\mathbf{C}}_{\mathbf{q}}^{b} + \dot{\mathbf{C}}_{\mathbf{s}}^{b}\dot{\mathbf{s}}^{k} + (\ddot{\mathbf{x}}^{ir})^{b}\Big] \end{aligned} \quad (37)$$

Substituting this result into the two first equations of the second time-derivative of the constraints (Equations a) one gets:

$$\begin{aligned} &\mathbf{C}_{\mathbf{q}}^{a}\ddot{\mathbf{q}}^{wi} - \mathbf{C}_{\mathbf{s}}^{a}(\mathbf{C}_{\mathbf{s}}^{b})^{-1}\Big[\mathbf{C}_{\mathbf{q}}^{b}\ddot{\mathbf{q}}^{wi} + \dot{\mathbf{C}}_{\mathbf{q}}^{b}\dot{\mathbf{q}}^{wi} + \dot{\mathbf{C}}_{\mathbf{s}}^{b}\dot{\mathbf{s}}^{k} + (\ddot{\mathbf{x}}^{ir})^{b}\Big] = -\dot{\mathbf{C}}_{\mathbf{q}}^{a}\dot{\mathbf{q}}^{wi} - \dot{\mathbf{C}}_{\mathbf{s}}^{a}\dot{\mathbf{s}}^{k} - (\ddot{\mathbf{x}}^{ir})^{a} \Rightarrow \\ &\Rightarrow \Big(\mathbf{C}_{\mathbf{q}}^{a} - \mathbf{C}_{\mathbf{s}}^{a}(\mathbf{C}_{\mathbf{s}}^{b})^{-1}\mathbf{C}_{\mathbf{q}}^{b}\Big)\ddot{\mathbf{q}}^{wi} = \\ &= -(\ddot{\mathbf{x}}^{ir})^{a} - \mathbf{C}_{\mathbf{s}}^{a}(\mathbf{C}_{\mathbf{s}}^{b})^{-1}(\ddot{\mathbf{x}}^{ir})^{b} - \Big(\dot{\mathbf{C}}_{\mathbf{q}}^{a} - \mathbf{C}_{\mathbf{s}}^{a}(\mathbf{C}_{\mathbf{s}}^{b})^{-1}\dot{\mathbf{C}}_{\mathbf{q}}^{b}\Big)\dot{\mathbf{q}}^{wi} - \Big(\dot{\mathbf{C}}_{\mathbf{s}}^{a} - \mathbf{C}_{\mathbf{s}}^{a}(\mathbf{C}_{\mathbf{s}}^{b})^{-1}\dot{\mathbf{C}}_{\mathbf{s}}^{b}\Big)\dot{\mathbf{s}}^{k} \end{aligned} \quad (38)$$

These are two constraint equations in which $\ddot{\mathbf{s}}^k$ does not appear. They can be augmented to the generalised force balance in the equations of motion. This equation can be written with a simplified notation as follows:

$$\mathbf{B}^{wi}\ddot{\mathbf{q}}^{wi} = -\mathbf{D}_{ir}^{wi} - \mathbf{E}^{wi}\dot{\mathbf{q}}^{wi} - \mathbf{G}^{wi}\dot{\mathbf{s}}^{k}, \quad (39)$$

where

$$\begin{aligned}
\mathbf{B}^{wi} &= \mathbf{C}^a_{\mathbf{q}} - \mathbf{C}^a_{\mathbf{s}}(\mathbf{C}^b_{\mathbf{s}})^{-1}\mathbf{C}^b_{\mathbf{q}},\\
\mathbf{D}^{wi}_{ir} &= -(\ddot{\mathbf{x}}^{ir})^a - \mathbf{C}^a_{\mathbf{s}}(\mathbf{C}^b_{\mathbf{s}})^{-1}(\ddot{\mathbf{x}}^{ir})^b,\\
\mathbf{E}^{wi} &= \dot{\mathbf{C}}^a_{\mathbf{q}} - \mathbf{C}^a_{\mathbf{s}}(\mathbf{C}^b_{\mathbf{s}})^{-1}\dot{\mathbf{C}}^b_{\mathbf{q}},\\
\mathbf{G}^{wi} &= \dot{\mathbf{C}}^a_{\mathbf{s}} - \mathbf{C}^a_{\mathbf{s}}(\mathbf{C}^b_{\mathbf{s}})^{-1}\dot{\mathbf{C}}^b_{\mathbf{s}}.
\end{aligned} \tag{40}$$

The term $\mathbf{D}^{wi}_{ir}$ is linear with respect to the second time-derivative of the irregularities. This term has little influence because the relatively high-wave length irregularities that are considered in rigid-body railway dynamics vary smoothly. In addition, it is a term that in practice is difficult to know accurately. Therefore, this term will be neglected in the following.

Considering all the developments shown in this chapter, the equations of motion of the railway vehicle in DAE-index 1 form yield:

$$\begin{bmatrix} \mathbf{M} & \mathbf{N}^T \\ \mathbf{B} & \mathbf{0} \end{bmatrix} \begin{bmatrix} \ddot{\mathbf{q}} \\ \boldsymbol{\lambda} \end{bmatrix} = \begin{bmatrix} \mathbf{Q} + \mathbf{Q}^{tang} \\ -\mathbf{E}\dot{\mathbf{q}} - \mathbf{G}\dot{\mathbf{s}} \end{bmatrix} \tag{41}$$

where $\mathbf{N}$, $\mathbf{B}$, $\mathbf{E}$ and $\mathbf{G}$ are the result of assembling the matrices $\mathbf{N}^{wi}$, $\mathbf{B}^{wi}$, $\mathbf{E}^{wi}$ and $\mathbf{G}^{wi}$ associated with all the wheelsets in the vehicle. Vector $\dot{\mathbf{s}}$ includes the profile parameters $\dot{\mathbf{s}}^k$ of all the wheelsets in the vehicle. To find the value of $\dot{\mathbf{s}}^k$, the first derivative of the constraint equations given in Eq. (34) has to be solved each time-step. This is a linear algebraic system of 4 equations and 2 unknowns. If the coordinates fulfil the KEC equations, the resulting linear system has to be compatible and it can be solved using the pseudo-inverse.

The calculation of the generalised tangential forces $\mathbf{Q}^{tang}$ follows the same procedure that was explained in Section 3.3.

5. Generation of lookup tables for flanging wheelsets

For the generation of contact lookup tables of wheelsets with wheel-rail profiles combination that show 2-point contact, this is, simultaneous contact in the tread and the flange, the procedure differs depending on whether these tables are going to be used with a hybrid method (explained in Section 3) or with a KEC-method (explained in Section 4). Recall that the KEC-method is an online contact method that requires the real wheel-rail contact problem to be solved first to find the equivalent profiles. In this context, Fig. 15 illustrates such difference between methods.

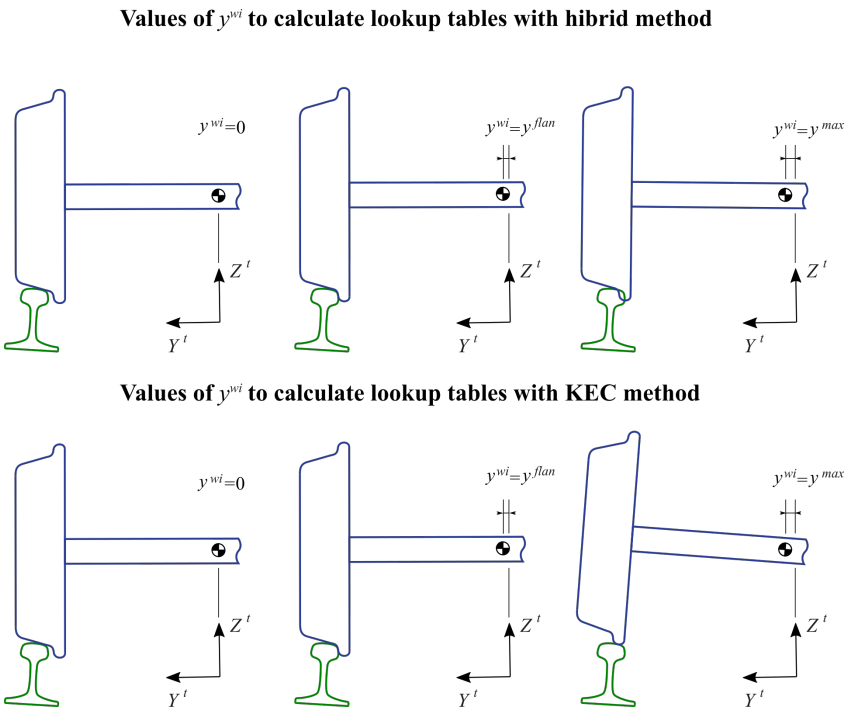

Fig. 15: Lateral displacement of wheels in the generation of lookup tables

Assume that, for the track with nominal gauge, the lateral displacement that produces 2-point contact is y^{flan}. Then, the range of values of y^{wi} for which the lookup table is calculated is $\begin{bmatrix} 0 & y^{max} \end{bmatrix}$, being $y^{max} > y^{flan}$. In the sub-range $y^{wi} \in \begin{bmatrix} 0 & y^{flan} \end{bmatrix}$ the lookup tables for both methods are equal. However, in the sub-range $y^{wi} \in \begin{bmatrix} y^{flan} & y^{max} \end{bmatrix}$ the lookup table for both methods differs.

In the case of lookup tables to be used with a hybrid method, the constraint contact on the tread is kept, allowing the wheel flange to penetrate the railhead. The location of the point of maximum indentation is stored in the lookup table to be used online as the flange contact point. In the case of the KEC-method, the constraint contact is moved to the flange, allowing the wheel tread to separate the railhead [27]. That way, the KEC-method accounts for the wheel climbing that is fundamental in simulation of derailment.

6. Simulation results

In this section, to analyse the differences between the lookup table and the KEC-method, a numerical comparison of three different case studies is presented: (1) simulation in irregular track with a wheel-rail profile combination that does not show 2-point contact, (2) simulation in irregular track with a wheel-rail profile combination that shows 2-point contact and (3) a wheelset climbing and derailment scenario with a wheel-rail profile combination that shows 2-point contact.

For all cases, a three-body suspended vehicle formed by two wheelsets and a bogie frame is analysed. The mass, inertia properties with respect to the wheelset and bogie frame are presented in Tab. 1. The primary suspension is modelled with four three-dimensional spring-damper elements per wheel

Tab. 1: Simulation parameters for the vehicle

Parameters	Model	Parameters	Model
Mass m^{wh} (kg)	1568	Inertia I^{wh} (kg·m^2)	656, 168, 656
Mass m^{b} (kg)	2982	Inertia I^{b} (kg·m^2)	1398.5, 2667, 2667

depicted in Fig. 16. These elements, that connect the axlebox to the bogie frame, have stiffness and damping properties defined in lateral, vertical and longitudinal direction as shown in Tab. 2. Also, Polach rolling contact theory [30] is used for tangential contact force computation.

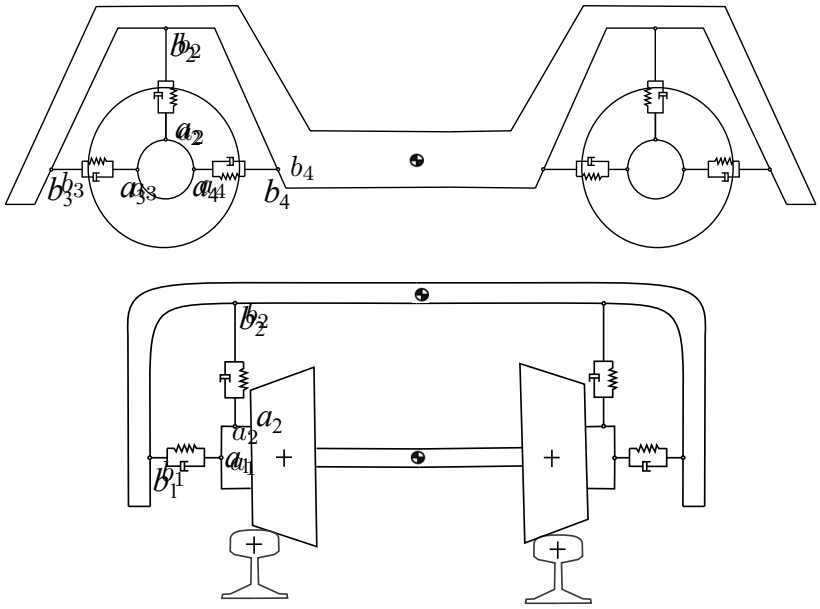

Fig. 16: One bogie with two wheelsets

Tab. 2: Primary suspension element used in the vehicle

Suspension element direction	Spring stiffness (kN/m)	Damping coeffi. (kN/m/s)	Suspension location	
			Axlebox	Bogie frame
Lateral	1500	45	a_1	b_1
Vertical	3000	67.5	a_2	b_2
Longitudinal	6000	90	a_3	b_3
Longitudinal	6000	90	a_4	b_4

Track irregularities are generated using analytical expressions of the power spectral density functions (PSD) [31]. The alignment, vertical profile, gauge variation and cross level are shown in Fig. 17.

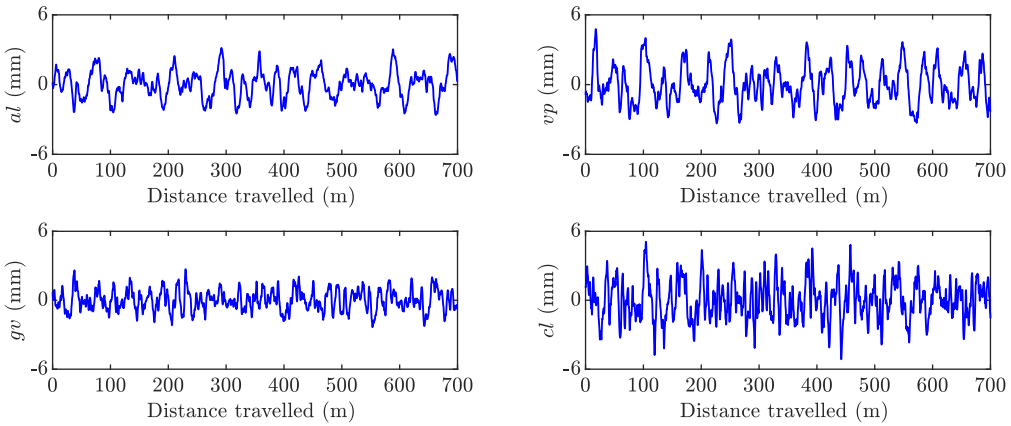

Fig. 17: Track irregularities, *al* is alignment, *vp* is vertical profile, *gv* is gauge variation, *cl* is cross level.

6.1. Simulation results in a track with irregularities with one point contact problem

The proposed first case study considers a wheel-rail profile combination that does not show 2-point contacts. It is simulated at a constant forward velocity of $V = 10$ m/s, in a 700-m track with irregularities formed by the following five segments: 100-m tangent, 50-m transition, 400-m left curve of $R = 235$ m radius segment, 50-m transition and 100-m tangent. The track geometry is shown in Fig. 18 where the different track segments limits are identified. This segment description is latter used in all simulation results figures. Wheel and rail profiles are shown Fig. 19. The parameters for both wheelset and the rail are in Tab. 3.

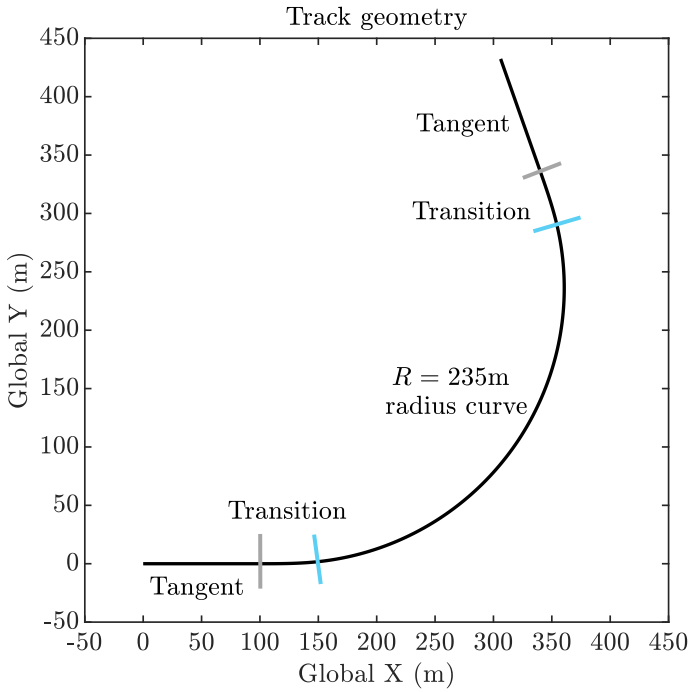

Fig. 18: Track geometry in solid dark line. Lines perpendicular to the track geometry refer to different track segments limits of tangent, transition and curve.

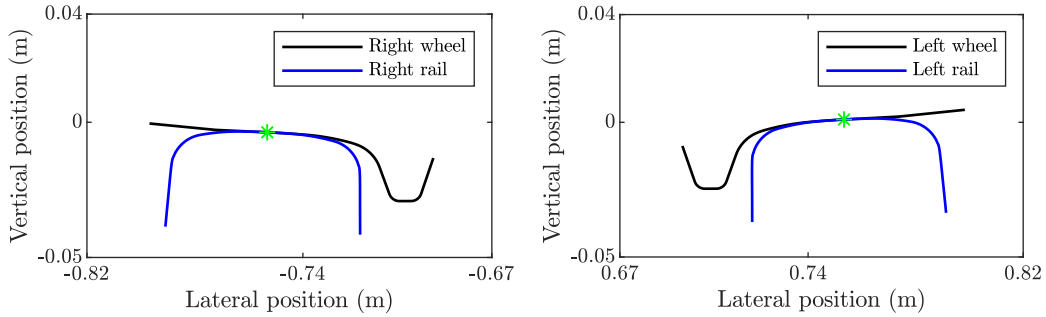

Fig. 19: Real wheel-rail profile combination which does not show two point contact.

Tab. 3: Simulation parameters for the wheelset which do not show 2-point contact

Parameters	Model	Parameters	Model	Parameters	Model	Parameters	Model
L_w (m)	0.7526	R_0 (m)	0.43	L_r (m)	0.7526	β (rad)	0.05

The relationship of transverse curve parameters between KEC equivalent and real wheel profiles can be found in Fig. 20. It can be seen that for each value of the equivalent parameter s^{lk}, only one contact point in the real profile s^{lw} can be obtained. This corresponds to a single point wheel-rail contact scenario.

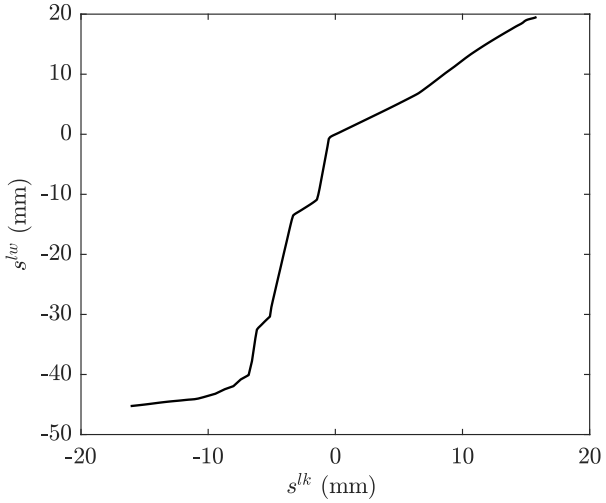

Fig. 20: Transverse curve parameters relation between KEC equivalent and real wheel profiles.

The comparison of lateral displacement and yaw angle for the wheelsets and bogie frame using lookup table and KEC-method is shown in Fig. 21. As it can be seen from the figures, the results of both approaches are almost identical. When the vehicle enters the curve, the frame takes negative values due to the curve negotiation, as it can observed in Fig. 21, without reaching a stable lateral position due to irregularities. This is also shown in Fig. 21 for the bodies yaw angle, where a maximum of 6 mrad at the front wheelset is obtained.

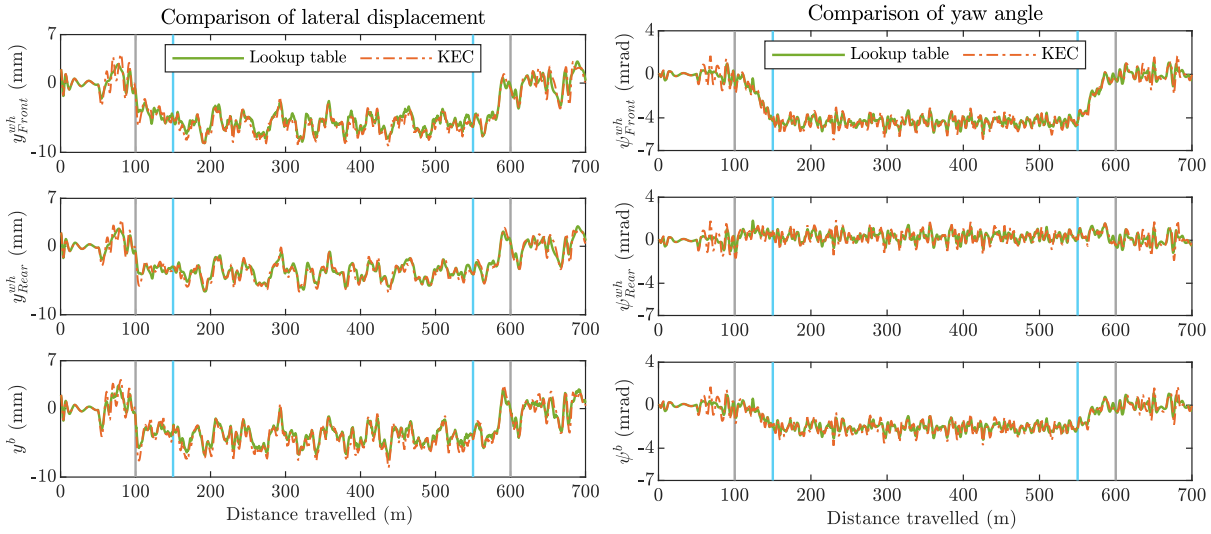

Fig. 21: Comparison of kinematics with the profiles which do not show two-point contact using both approaches. Left: lateral displacement, Right: yaw angle. Full vertical lines refer to the limits of track segments as shown in Fig. 18.

Fig. 22 and Fig. 23 show the comparison of normal contact forces at front and rear wheelsets using both approaches . Since there is always an unique contact point per wheel-rail pair, normal contact forces of both approaches are treated as reaction forces using Eq. (23). In this context, the results from both approaches are very close to each other. When the vehicle negotiates the left curve,

right wheel for both wheelsets experiences a higher normal contact force than left one, which has identical behaviour as in [18].

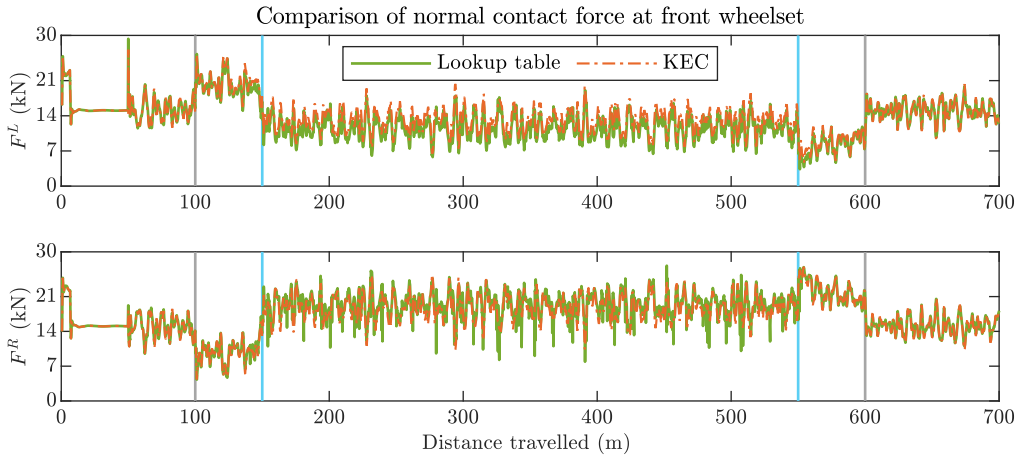

Fig. 22: Comparison of normal contact forces at front wheelset using both approaches.

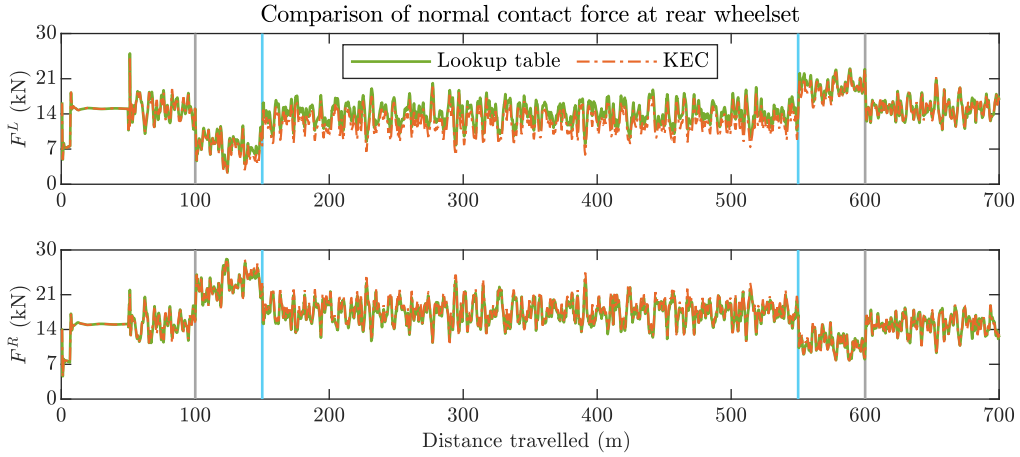

Fig. 23: Comparison of normal contact forces at rear wheelset using both approaches. Solid lines: solution with lookup tables.

6.2. Simulation results in a track with irregularities with two point contact problem

The second case study is the same bogie vehicle whose wheelsets use a wheel-rail profile combination that shows two-point contacts. The vehicle is assumed to have a constant forward velocity of $V = 10$ m/s along the same 700-m length track with irregularities shown in Fig. 18. Wheel and rail profiles are shown in Fig. 24. The parameters for the wheelset and the rail are given in Tab. 4.

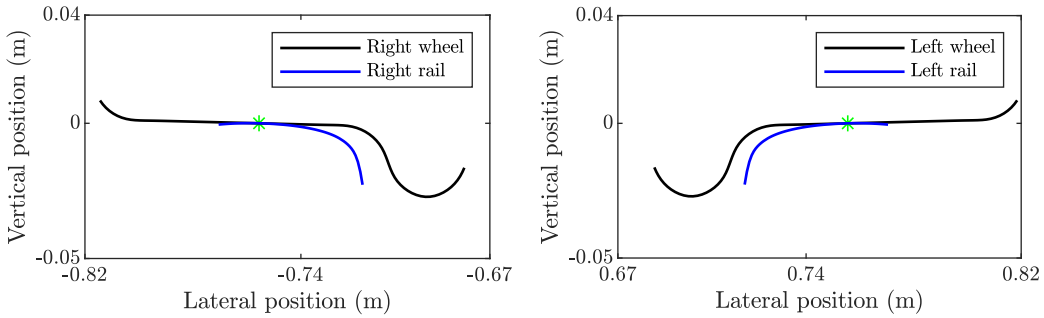

Fig. 24: Real wheel-rail profile combination which shows two point contact

Tab. 4: Parameters for the wheel-rail profile combination which can show two point contact

Parameters	Model	Parameters	Model	Parameters	Model	Parameters	Model
L_w (m)	0.7515	R_0 (m)	0.457	L_r (m)	0.7555	β (rad)	0

Fig. 25 plots the location of the contact points in the real profile as a function of the location of the contact point in the KEC-equivalent profile. It can be seen that for a certain value of the equivalent parameter s^{lk} there are two simultaneous contact points in the real profile s^{lw}. This corresponds to a two-point wheel-rail contact scenario where one contact point is located at the tread s_t^{lw}, and another one is located at the flange s_f^{lw}. Based on the parameters given in [27] to efficiently use the KEC-method with the two-point contact scenario, this relation between the equivalent and real wheel profiles is regularised as a dashed green line in Fig. 25. This allows a continuous contact point evolution from tread to flange avoiding the discontinuities associated with the contact constraints. However, Fig. 25 is not completely used for the lookup table approach, since only tread contact is considered. Instead, an compliant lateral force model is considered to account for wheel penetration at the flange, as shown in Sec. 5.

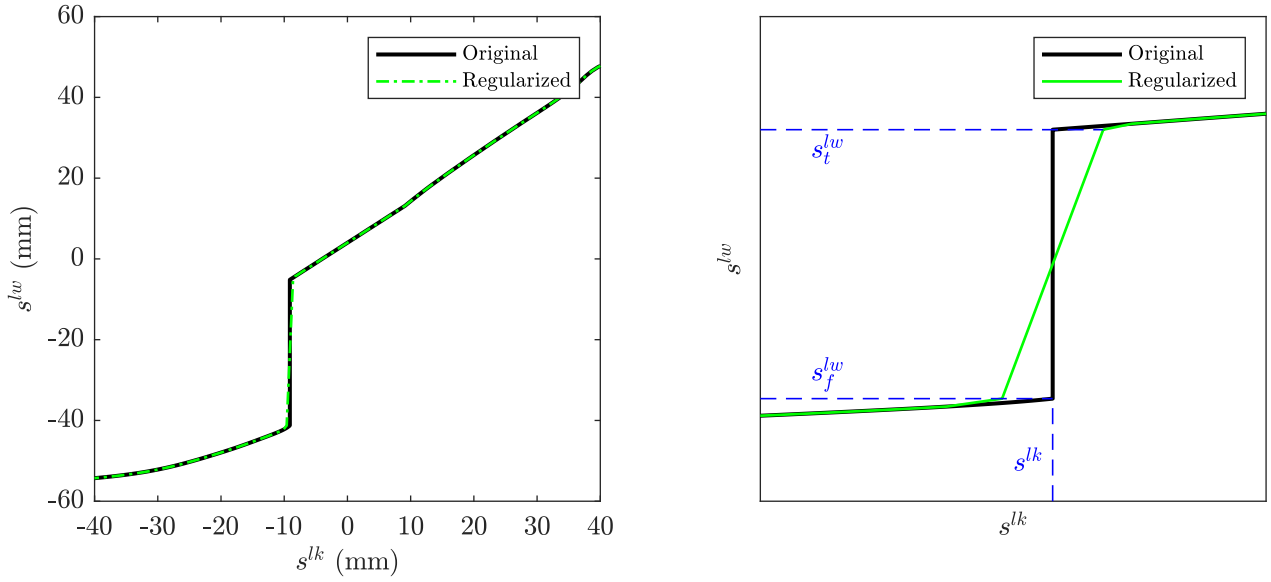

Fig. 25: Regularisation of the transverse curve parameter relation for the left equivalent and real wheels when KEC-method is used

The lateral displacement and the yaw angle of both wheelsets are compared in Fig. 26. The resulting lateral displacements are quite similar using both approaches. However, when the vehicle enters into the 235 m radius curve, flange contacts occurs. The lateral displacement y^{wh} enters into the sub-range $y^{wh} \in \left[y^{flan} \quad y^{max}\right]$, in which the kinematic of yaw angle for both methods differs (see Fig. 15 in Sec. 5). However, as it can be seen in Fig. 26, the lateral displacement of the vehicle bodies is very similar in this particular problem. Slight differences can be observed in the yaw angles shown in Fig. 26.

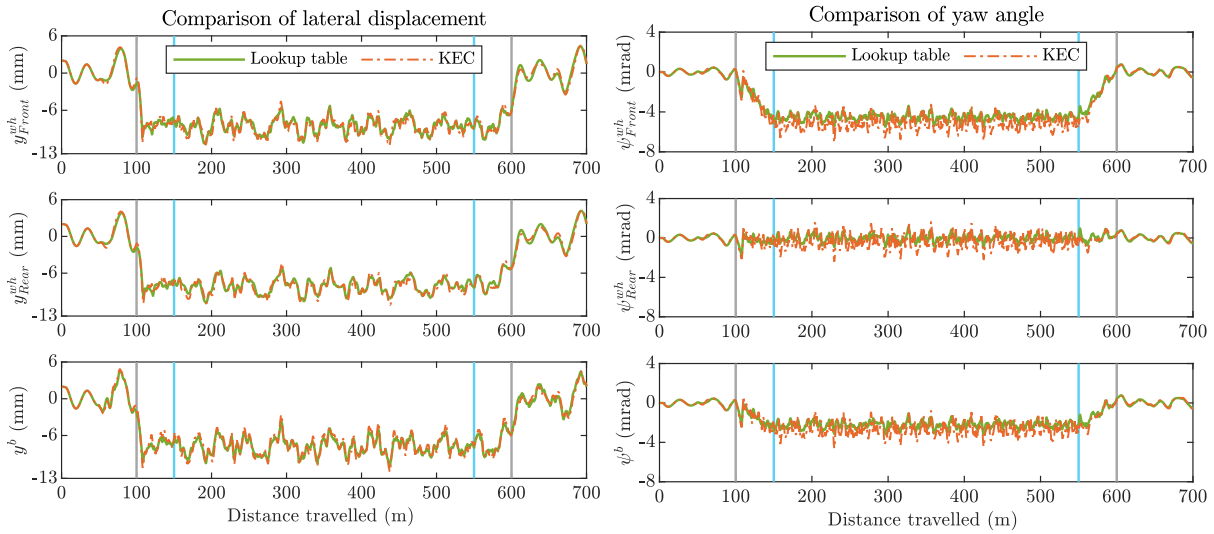

Fig. 26: Comparison of kinematics using profiles that show two-point contacts. Left: lateral displacement, Right: yaw angle

Fig. 27 and Fig. 28 show the comparison of the normal contact force at right wheel of front and rear wheelset using both approaches. The normal contact forces at the right tread and flange differ when the wheelset is negotiating the curve. That is due to the two different contact approaches (constrained in the KEC-method, elastic in the lookup table method) used in the wheel flange area. Fig. 29 shows the simulated flange indentations in the right wheel of the front and rear wheelsets with the Hertzian parameters are $K_{hertz} = 1 \cdot 10^{10}$ kN/m$^{1.5}$ and $C_{damp} = 1 \cdot 10^{8}$ kN/m/s.

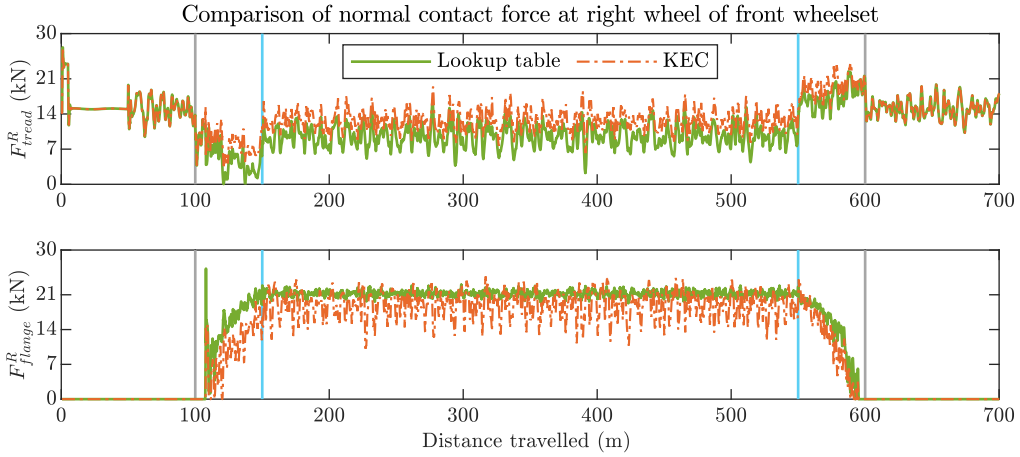

Fig. 27: Comparison of normal contact forces at front wheelset with two-point contacts.

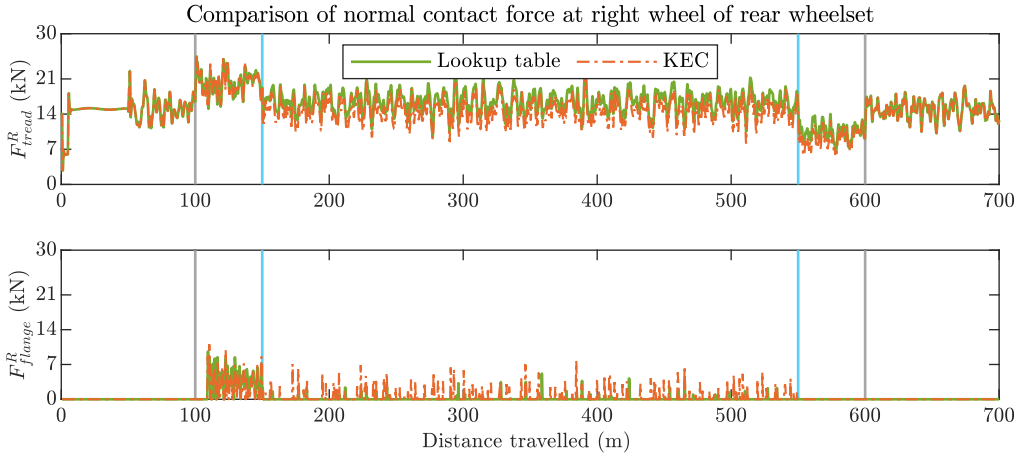

Fig. 28: Comparison of normal contact forces at rear wheelset with two-point contacts.

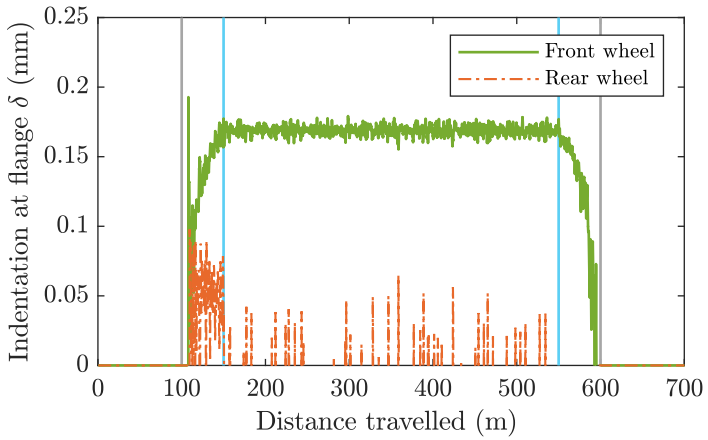

Fig. 29: Indentation at right flange using lookup table approach.

6.3. Wheelset climbing and derailment with 2-point wheel-rail profile combination

When the vehicle is running with a high forward velocity or on a small radii curve, wheelset climbing and derailment may occur. That is the purpose of this case study, where the bogie vehicle is running at a constant forward velocity of $V = 25$ m/s on a 1000-m track without irregularities, formed by the following five segments: 100-m tangent, 50-m transition, 350-m left curve of R = 100 m radius segment, 150-m transition and 350-m tangent. The Hertzian parameters for the flange contact using the lookup table approach are the same as in the previous case study. This is, $K_{hertz} = 1 \cdot 10^{10}$ N/m$^{1.5}$ and $C_{damp} = 1 \cdot 10^{8}$ N/m/s.

The comparison of the lateral and vertical displacement using both approaches is shown in Fig. 30. When using the lookup table approach, the lateral displacement reaches the steady motion due to permanent flange contact. As a result, the vertical displacement keeps constant during the simulation. However, the penetration obtained using this approach depends on the Hertzian parameters used, which may give high values that are not realistic, as shown in Fig. 31. However, when using the KEC-method, the wheelset vertical displacement at Fig. 30 shows that the wheelset tends to climb several times when it starts to enter into transitions at around 100 m. Due to regularised tread-flange transition used in KEC-method, the rear flange climbs when passing through the small curve and the derailment occurs when the longitudinal coordinate is approximately 380 m.

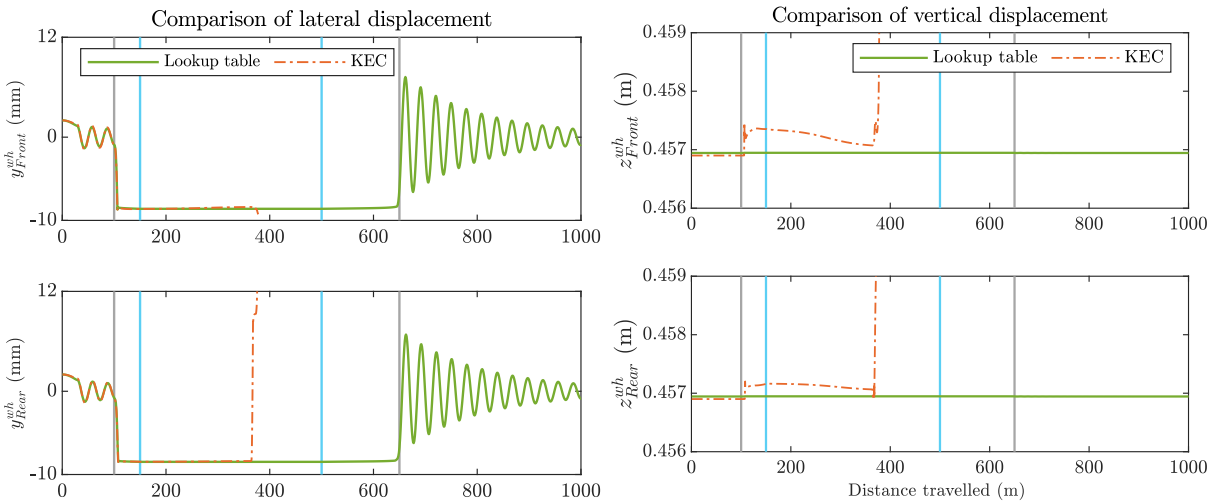

Fig. 30: Comparison of kinematics at wheel-climbing scenario using profiles that show two-point contacts. Left: lateral displacement, Right: vertical displacement

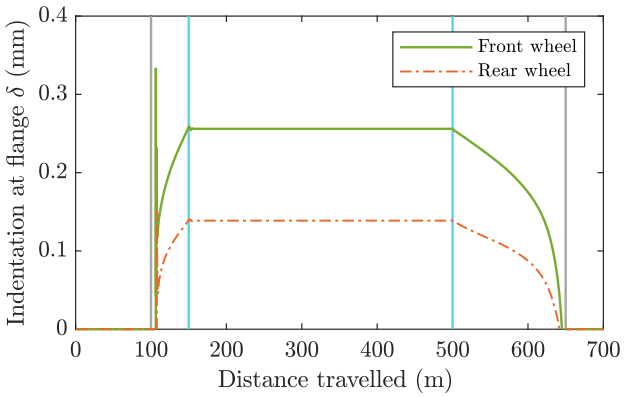

Fig. 31: Indentation at right flange using the lookup table approach

The comparison of yaw angle using the lookup table and KEC-method is shown in Fig. 32. When the wheelset is passing through the 100 m radius curved segment, small values of yaw angle are obtained using the lookup table approach, while higher values are produced with the KEC-method approach due to the wheel climb.

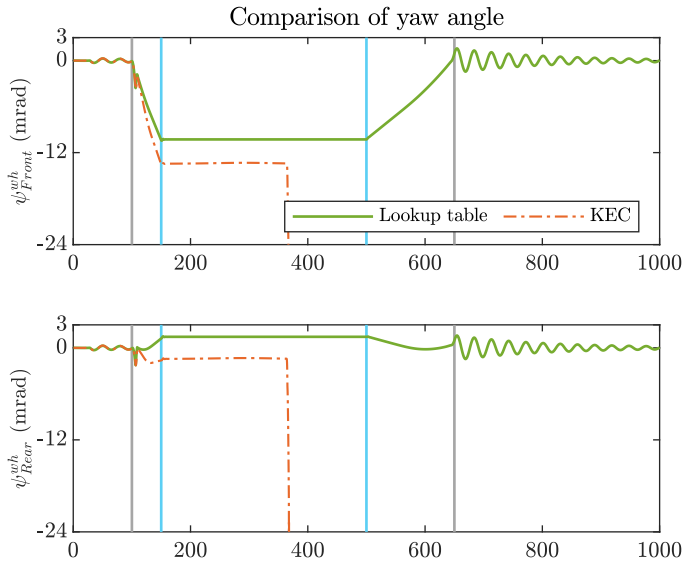

Fig. 32: Comparison of wheelsets yaw angle using both approaches at the wheel climbing scenario

Finally, Fig. 33 shows the wheelset climbing scenario during the simulation. Accordingly, the configurations of the rear left wheel in the contact point section during the simulation is shown in the same figure with different wheelset lateral displacements. It is observed that the rear left wheel is climbing the rail with one distinct jumps in contact point. The contact point on the wheel tread which is in contact with the top of the rail is jumped to the rail corner, in which wheel flange is in contact. As the lateral displacement increases, the wheel is completely moved up to the top of the rail. This scenario agrees with the results proposed in [23].

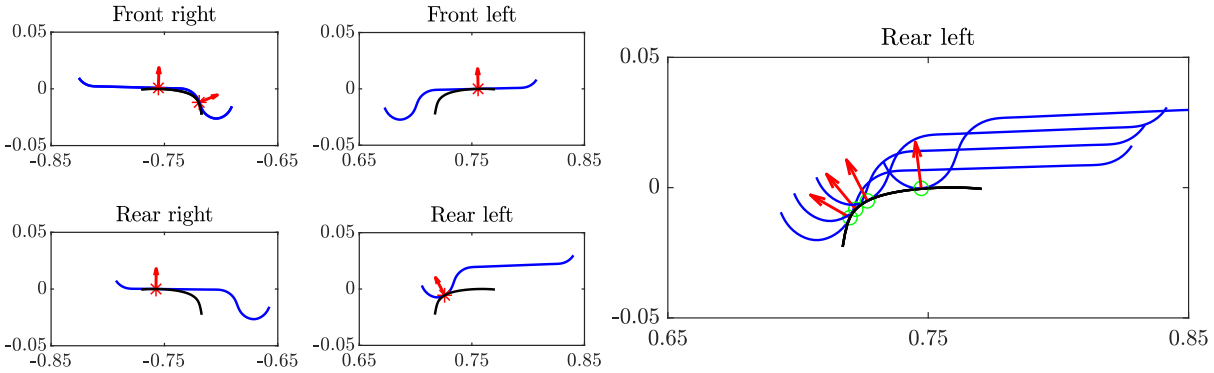

Fig. 33: Frames of the wheelsets during wheelset climbing using KEC approach (Left); Wheel/rail contact in point section with different wheelset lateral displacement during the simulation (Right)

In this example, the lookup method and the KEC-method result in totally different behaviour of the vehicle. As it has been shown, simulations based on the hybrid-lookup table method may produce results that are not in the safe side, because wheel climbing cannot be.

7. Selection of the flange contact stiffness

There is a very important parameter that controls the simulations with the lookup table method. This parameter is the flange contact stiffness. The selection of a large value of the contact stiffness, for example the one that results from the application of the Hertz contact theory, results in simulations that require to reduce the time-step to very low values to keep the system stability. Because flange contact is an event that appears suddenly as an impact, in the best cases, simulations slow down tremendously any time flange contact occurs. In these conditions, the resulting flange normal contact forces are so high that they can be considered as physically inadmissible. Hertzian stiffness is actually much higher than the real one, because it only accounts for local deformation effects, without considering the structural deformation of the wheel, that is specially important when the load is applied transversely at the flange. The comparison of the computational efficiency with both approaches is shown in Tab. 5. Along the different stiffness used for the flange contact, the one that results in applying directly the Hertz contact theory is within the range $1 \cdot 10^{12} - 1 \cdot 10^{13}$ $\mathrm{N/m^{1.5}}$. Such high values of contact stiffness increase the computational effort and might lead integrators to stall during the simulation, as shown in Tab. 5. The code has been written in Matlab and run on an Intel Core i5 laptop with a 2.5 GHz CPU, 32 GB of RAM and Microsoft Windows. The variable time step integrator of *ode15s*, is used for the dynamic simulation. The total simulation time is 70 s with a maximum time step of $\Delta t = 1$ ms.

Tab. 5: CPU time per 1s simulation of the second case study in Sec. 6.2

	Lookup table					KEC
Flange contact stiffness ($\mathrm{N/m^{1.5}}$)	$1 \cdot 10^{13}$	$1 \cdot 10^{12}$	$1 \cdot 10^{11}$	$1 \cdot 10^{10}$	$1 \cdot 10^{9}$	
CPU time (s)	Stall	11.8	6.9	2.45	1.09	4.4
Function evaluation	Stall	153338	81265	20901	11822	59299

If the selected contact stiffness is low, simulations are relatively smooth even with multiple flange contacts. The dynamicist may be tempted to use low value of the stiffness just to get any simulation results, or to get them in a reasonable period of time. These results may show flange to rail-head indentations so large that they can be considered as physically inadmissible, but vehicle motion appears to be stable (see indentations in Fig. 34 with different contact stiffness). As a conclusion, on the one hand, the selection of the contact stiffness is fundamental in the simulation of wheel flange contact with a hybrid method and, on the other hand, this selection is some-how arbitrary when not much information is known about the local contact process and the wheel structural deformation. Due to these reasons, it is preferable to use a method that do not use a flange contact stiffness, treats equally the tread and the flange contacts, results in smooth simulations even with multiple flange contacts and it is able to simulate wheel climbing. The KEC-method fulfils these conditions.

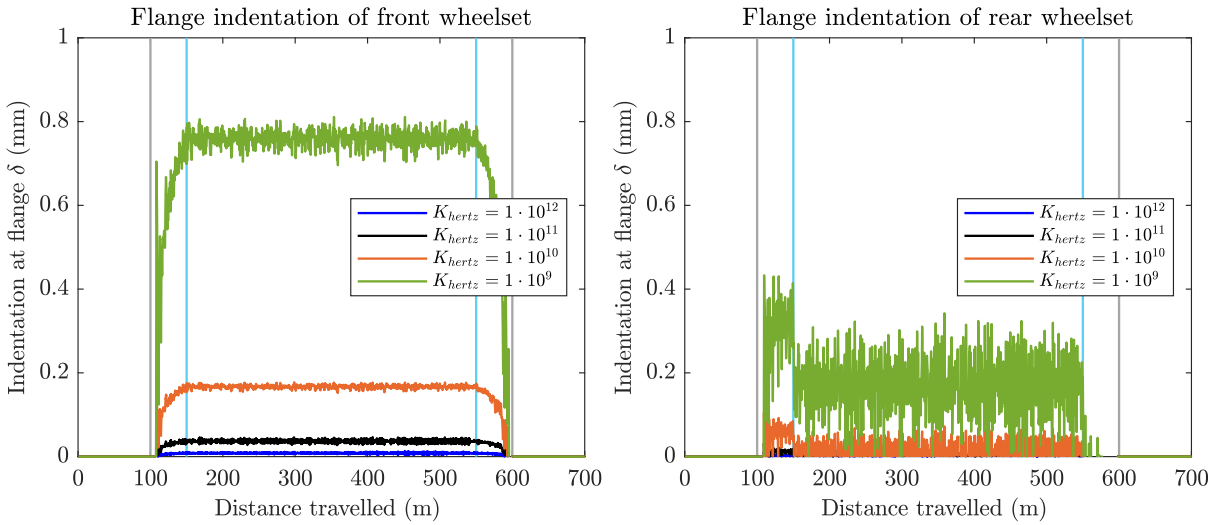

Fig. 34: Flange to rail-head indentations at front and rear wheelsets with different flange contact stiffness of the second case study in Sec. 6.2. The unit of flange contact stiffness K_{herz} is $\mathrm{N/m^{1.5}}$.

8. Conclusion

Two constraint-based formulations for the wheel-rail contact simulation in multibody dynamics are introduced and compared: the use of precalculated contact lookup tables and the Knife-edge Equivalent Contact method (KEC-method). Contact simulation with lookup tables is a well-known and widely used technique. This paper describes a method that does not consider the influence of the yaw angle in the contact geometry. This approach, that is sufficiently accurate in most scenarios, is commonly improved in most simulation codes by including the wheelset yaw as an additional entry to the lookup tables. Regarding this method, the original contributions of this paper are: (1) a method for interpolating the tables in the presence of irregularities and (2) a method for the calculation of the normal contact forces that does not require the use of the Jacobian of the wheel-rail contact constraints. This method models the wheel-rail flange contact using an elastic approach to be able to simulate the two-point contact scenario. That is why this method is considered as a hybrid approach.

The KEC-method is a new wheel-rail contact approach recently developed by the authors. The KEC-method substitutes the real wheel and rail profiles with a fictitious wheel profile that contacts a spatial curve such that the relative wheel-track motion remains unchanged. This method results in very important advantages for the simulations: (1) the contact constraints are very simple and can be solved on-line, (2) constraint functions are continuous even in the case of two-point contact, (3) it allows a smooth transition of the contact force from the wheel-tread to the wheel-flange and (4) it is effective in the simulation of wheel climbing. This is the only constraint-based contact method that can be used to simulate the two-point wheel rail contact. Regarding this method, the main contribution of this paper is to show that the wheel KEC-equivalent profile, that is generated using an irregularity-free track section, remains valid, this is, keeps the same space of allowable motion, also in the presence of track irregularities.

Three different case studies of a bogie vehicle with different wheel-rail profile combinations in a tangent and curved track are examined. Results show that, in general, both approaches provide

a similar dynamic behaviour and normal contact forces. Due to the differences in the simulation of flange contact, the wheelsets yaw angle differs at curve negotiation. However, when simulating the negotiation of a curve at relatively high velocity, the results of both methods are drastically different. Due to its ability to simulate wheel climbing, the KEC-method predicts derailment while the lookup-hybrid method predicts a permanent and stable flange contact, even in the presence of track irregularities. It can be concluded that simulations with the lookup-hybrid method may not be on the safe side and the KEC-method can be considered as superior when doing safety analysis.

Acknowledgements

The first and third authors thank the Department of Economy, Science, Enterprise and University of the Andalusian Regional Government, in Spain, under the PAIDI 2020 program with project reference P18-RT-1772. The second author thanks for the support given by Business of Finland under the SmartTram-LUT project with reference 6292/31/2018. All this support is gratefully acknowledged.

Conflicts of interest

The authors declare that there is no conflict of interest to this work.

References

[1] S. Bruni, J. Meijaard, G. Rill, A. Schwab, State-of-the-art and challenges of railway and road vehicle dynamics with multibody dynamics approaches, Multibody Syst Dyn 49 (2020) 1–32.

[2] S. Z. Meymand, A. Keylin, M. Ahmadian, A survey of wheel–rail contact models for rail vehicles, Vehicle System Dynamics 54 (3) (2016) 386–428. doi:10.1080/00423114.2015.1137956.

[3] A. A. Shabana, M. Tobaa, H. Sugiyama, K. E. Zaazaa, On the computer formulations of the wheel/rail contact problem, Nonlinear Dynamics 40 (2) (2005) 169–193. doi:10.1007/s11071-005-5200-y.

[4] A. A. Shabana, K. E. Zaazaa, J. L. Escalona, J. R. Sany, Development of elastic force model for wheel/rail contact problems, Journal of Sound and Vibration 269 (1–2) (2004) 295–325. doi:https://doi.org/10.1016/S0022-460X(03)00074-9.

[5] M. Machado, P. Moreira, P. Flores, H. M. Lankarani, Compliant contact force models in multibody dynamics: Evolution of the hertz contact theory, Mechanism and Machine Theory 53 (2012) 99–121.

[6] P. Flores, H. M. Lankarani, Contact force models for multibody dynamics, Vol. 226, Springer, 2016.

[7] A. A. Shabana, J. R. Sany, An augmented formulation for mechanical systems with non-generalized coordinates: application to rigid body contact problems, Nonlinear dynamics 24 (2) (2001) 183–204. doi:10.1023/A:1008362309558.

[8] H. Sugiyama, Y. Suda, On the contact search algorithms for wheel/rail contact problems, Journal of computational and nonlinear dynamics 4 (4).

[9] F. Marques, H. Magalhães, J. Pombo, J. Ambrósio, P. Flores, A three-dimensional approach for contact detection between realistic wheel and rail surfaces for improved railway dynamic analysis, Mechanism and Machine Theory 149 (2020) 103825.

[10] H. Magalhães, F. Marques, B. Liu, P. Antunes, J. Pombo, P. Flores, J. Ambrósio, J. Piotrowski, S. Bruni, Implementation of a non-hertzian contact model for railway dynamic application, Multibody System Dynamics 48 (1) (2020) 41–78.

[11] J. Pombo, J. Ambrósio, M. Silva, A new wheel–rail contact model for railway dynamics, Vehicle System Dynamics 45 (2) (2007) 165–189. doi:https://doi.org/10.1080/00423110600996017.

[12] J. Pombo, J. Ambrósio, Application of a wheel–rail contact model to railway dynamics in small radius curved tracks, Multibody System Dynamics 19 (2008) 91–114. doi:https://doi.org/10.1007/s11044-007-9094-y.

[13] J. Pombo, J. Ambrósio, An alternative method to include track irregularities in railway vehicle dynamic analyses, Nonlinear Dynamics 68 (2012) 161–176. doi:https://doi.org/10.1007/s11071-011-0212-2.

[14] M. Malvezzi, E. Meli, S. Falomi, A. Rindi, Determination of wheel–rail contact points with semianalytic methods, Multibody System Dynamics 20 (4) (2008) 327–358. doi:10.1007/s11044-008-9123-5.

[15] S. Falomi, M. Malvezzi, E. Meli, Multibody modeling of railway vehicles: Innovative algorithms for the detection of wheel–rail contact points, Wear 271 (1-2) (2011) 453–461. doi:https://doi.org/10.1016/j.wear.2010.10.039.

[16] L. Baeza, D. J. Thompson, G. Squicciarini, F. D. Denia, Method for obtaining the wheel–rail contact location and its application to the normal problem calculation through 'CONTACT', Vehicle System Dynamics 56 (11) (2018) 1734–1746. doi:10.1080/00423114.2018.1439178.

[17] S. Muñoz, J. F. Aceituno, P. Urda, J. L. Escalona, Multibody model of railway vehicles with weakly coupled vertical and lateral dynamics, Mechanical Systems and Signal Processing 115 (2019) 570–592. doi:10.1016/j.ymssp.2018.06.019.

[18] J. L. Escalona, J. F. Aceituno, P. Urda, O. Balling, Railway multibody simulation with the knife-edge-equivalent wheel–rail constraint equations, Multibody System Dynamics (2019) 1–30doi:10.1007/s11044-019-09708-x.

[19] J. L. Escalona, J. F. Aceituno, Multibody simulation of railway vehicles with contact lookup tables, International Journal of Mechanical Science 155 (2019) 571–582. doi:https://doi.org/10.1016/j.ijmecsci.2018.01.020.

[20] M. Bozzone, E. Pennestrì, P. Salvini, A lookup table-based method for wheel–rail contact analysis, Proceedings of the Institution of Mechanical Engineers, Part K: Journal of Multi-body Dynamics 225 (2) (2011) 127–138.

[21] J. Santamaría, E. G. Vadillo, J. Gómez, A comprehensive method for the elastic calculation of the two-point wheel–rail contact, Vehicle System Dynamic 44 (sup1) (2006) 240–250. doi:https://doi.org/10.1080/00423110600870337.

[22] H. Sugiyama, K. Araki, Y. Suda, On-line and off-line wheel/rail contact algorithm in the analysis of multibody railroad vehicle systems, Journal of Mechanical Science and Technology 23 (2009) 991–996. doi:https://doi.org/10.1007/s12206-009-0327-2.

[23] H. Sugiyama, T. Sekiguchi, R. Matsumura, S. Yamashita, Y. Suda, Wheel/rail contact dynamics in turnout negotiations with combined nodal and non-conformal contact approach, Multibody System Dynamics 27 (2012) 55–74. doi:https://doi.org/10.1007/s11044-011-9252-0.

[24] J. Piotrowski, B. Liu, S. Bruni, The kalker book of tables for non-hertzian contact of wheel and rail, Vehicle System Dynamics 55 (6) (2017) 875–901.

[25] F. Marques, H. Magalhães, B. Liu, J. Pombo, P. Flores, J. Ambrósio, J. Piotrowski, S. Bruni, On the generation of enhanced lookup tables for wheel-rail contact models, Wear 434–435 (2019) 202993. doi:https://doi.org/10.1016/j.wear.2019.202993.

[26] J. Piotrowski, S. Bruni, B. Liu, E. D. Gialleonardo, A fast method for determination of creep forces in non-Hertzian contact of wheel and rail base on a book of tables, Multibody System Dynamics 45 (2019) 169–184. doi:https://doi.org/10.1007/s11044-018-09635-3.

[27] J. F. Aceituno, P. Urda, E. Briales, J. L. Escalona, Analysis of the two-point wheel-rail contact scenario using the knife-edge-equivalent contact constraint method, Mechanism and Machine Theory 148 (2020) 103803. doi:https://doi.org/10.1016/j.mechmachtheory.2020.103803.

[28] J. Kalker, Three dimensional elastic bodies in rolling contact, Kluwer Academic Publishers, Dordrecht/-Boston/London, 1990.

[29] O. Polach, Creep forces in simulations of traction vehicles running on adhesion limit, Wear 258 (7-8) (2005) 992–1000. doi:10.1016/j.wear.2004.03.046.

[30] O. Polach, A fast wheel-rail forces calculation computer code, Vehicle System Dynamics 33 (sup1) (1999) 728–739. doi:10.1080/00423114.1999.12063125.

[31] H. Claus, W. Schiehlen, Modeling and simulation of railway bogie structural vibrations, Vehicle System Dynamics 29 (1998) 538–552. doi:10.1080/00423119808969585.